

University of Windsor

Scholarship at UWindor

Electronic Theses and Dissertations

Theses, Dissertations, and Major Papers

1-1-2007

Preliminary empirical and modeling analyses for model based diesel engine control.

Yuyu Tan

University of Windsor

Follow this and additional works at: <https://scholar.uwindsor.ca/etd>

Recommended Citation

Tan, Yuyu, "Preliminary empirical and modeling analyses for model based diesel engine control." (2007). *Electronic Theses and Dissertations*. 7170.

<https://scholar.uwindsor.ca/etd/7170>

This online database contains the full-text of PhD dissertations and Masters' theses of University of Windsor students from 1954 forward. These documents are made available for personal study and research purposes only, in accordance with the Canadian Copyright Act and the Creative Commons license—CC BY-NC-ND (Attribution, Non-Commercial, No Derivative Works). Under this license, works must always be attributed to the copyright holder (original author), cannot be used for any commercial purposes, and may not be altered. Any other use would require the permission of the copyright holder. Students may inquire about withdrawing their dissertation and/or thesis from this database. For additional inquiries, please contact the repository administrator via email (scholarship@uwindsor.ca) or by telephone at 519-253-3000ext. 3208.

Preliminary Empirical and Modeling Analyses for Model Based Diesel Engine Control

by
Yuyu Tan

A Thesis
Submitted to the Faculty of Graduate Studies
through Mechanical, Automotive and Materials Engineering
in Partial Fulfillment of the Requirements for
the Degree of Master of Applied Science at the
University of Windsor

Windsor, Ontario, Canada

July 2007

© 2007 Yuyu Tan



Library and Archives
Canada

Published Heritage
Branch

395 Wellington Street
Ottawa ON K1A 0N4
Canada

Bibliothèque et
Archives Canada

Direction du
Patrimoine de l'édition

395, rue Wellington
Ottawa ON K1A 0N4
Canada

Your file *Votre référence*
ISBN: 978-0-494-62752-5
Our file *Notre référence*
ISBN: 978-0-494-62752-5

NOTICE:

The author has granted a non-exclusive license allowing Library and Archives Canada to reproduce, publish, archive, preserve, conserve, communicate to the public by telecommunication or on the Internet, loan, distribute and sell theses worldwide, for commercial or non-commercial purposes, in microform, paper, electronic and/or any other formats.

The author retains copyright ownership and moral rights in this thesis. Neither the thesis nor substantial extracts from it may be printed or otherwise reproduced without the author's permission.

In compliance with the Canadian Privacy Act some supporting forms may have been removed from this thesis.

While these forms may be included in the document page count, their removal does not represent any loss of content from the thesis.

AVIS:

L'auteur a accordé une licence non exclusive permettant à la Bibliothèque et Archives Canada de reproduire, publier, archiver, sauvegarder, conserver, transmettre au public par télécommunication ou par l'Internet, prêter, distribuer et vendre des thèses partout dans le monde, à des fins commerciales ou autres, sur support microforme, papier, électronique et/ou autres formats.

L'auteur conserve la propriété du droit d'auteur et des droits moraux qui protègent cette thèse. Ni la thèse ni des extraits substantiels de celle-ci ne doivent être imprimés ou autrement reproduits sans son autorisation.

Conformément à la loi canadienne sur la protection de la vie privée, quelques formulaires secondaires ont été enlevés de cette thèse.

Bien que ces formulaires aient inclus dans la pagination, il n'y aura aucun contenu manquant.


Canada

ABSTRACT

Previous work indicates that low temperature combustion (LTC) modes, including homogeneous charge compression ignition (HCCI) cycles, are capable of reducing nitrogen oxides and soot simultaneously in diesel engines. However, such combustion modes are less robust than the conventional diesel combustion and have a narrower range of stable engine operation. In addition, in cases of diesel HCCI cycles, the combustion process may even occur before the piston completes the compression stroke, which may cause excessive efficiency reduction and combustion roughness. To improve the diesel low temperature combustion engine performance, preliminary analyses have been made to identify the major parameters that affect engine thermal efficiency. The impact of heat release phasing, duration, shaping, and splitting on the thermal efficiency has been analyzed with zero-dimensional (zero-D) engine cycle simulations. The correlations between the cylinder pressure and the heat release curves have been characterized to facilitate model based control. Additionally, independent and high precision controls on the rate of exhaust gas recirculation (EGR) flow and the fuel injection pressure of the common-rail system have been implemented and tested in this research. A variety of algorithms have been proposed and programmed to improve the response and precision of the EGR valve and the rail pressure in both manual and automatic modes. The present work targets to develop cylinder pressure based adaptive fuel-injection control strategies that will be used to stabilize the engine operation during the low-temperature combustion modes.

LIST OF PUBLICATIONS

Ming Zheng, **Yuyu Tan**, Mwila Clarence Mulenga, and Meiping Wang, “Thermal Efficiency Analyses of Diesel Low Temperature Combustion Cycles”, accepted for publication at SAE Powertrain & Fluid Systems Conference and Exhibition 2007 (Technical Session: Engine Controls), Chicago, USA, SAE paper No. 07FFL-10, p.11.

Ming Zheng, Graham T Reader, **Yuyu Tan** and Meiping Wang, “Adaptive Combustion Control to Improve Diesel HCCI Cycle Fuel Efficiency”, submitted to ASME-ICE 2007 Fall Technical Conference, October 14-17, 2007, Charleston, South Carolina, USA, ASME paper No. ICEF2007-1630, p.9.

Yuyu Tan, Mwila Clarence Mulenga, Usman Asad, Meiping Wang, Graham T. Reader and Ming Zheng, “Preliminary Analysis of Fuel Efficiency of Diesel HCCI Cycles”, Combustion Institute / Canadian Section, Spring Technical Meeting, Banff, AB, Canada, May 13-16, 2007, **presenter**, Session-D3, pp.1-8.

Ming Zheng, Mwila Clarence Mulenga, Graham T. Reader, **Yuyu Tan**, and Meiping Wang, Jimi Tjong, “Neat Biodiesel Fuel Engine Tests and Preliminary Modelling”, SAE 2007 World Congress, paper No. 2007-01-0616, SP2067, p.14.

Mwila Clarence Mulenga, Ming Zheng, Graham T. Reader, David S-K. Ting, **Yuyu Tan**, Usman Asad, and Meiping Wang, “Investigating EGR on Low-Temperature Combustion NO_x and PM in Diesel Engines”, Combustion Institute / Canadian Section, Spring Technical Meeting, Waterloo, ON, Canada, May 14-17, 2006, Session-L1, pp.1-8.

DEDICATION

To my beloved,

Chao Liu.

ACKNOWLEDGEMENTS

I would like to express my sincere gratitude to my supervisors, Dr. Ming Zheng and Dr. Graham T. Reader, for their constant help and encouragement throughout this work, and for their invaluable guidance and understanding throughout my study in the Master's degree program.

I also wish to thank my committee members Dr. Xiaohong Xu and Dr. Jimi Tjong for their advice in this research.

My appreciation is also extended to my colleagues in Clean Diesel Engine Laboratory: Dr. Meiping Wang for her constant encouragement and constructive criticism; Mwila Clarence Mulenga for his continuous encouragement and great help especially in writing; Raj Kumar for his helpful discussions; Usman Asad for his quick technical insights and valuable inspiring; Siddhartha Banerjee for his constant help; Xiaoye Han for the experimental setup; and William Bombardier, Suek Jin Ko and Martin Kobler for their helpful assistance. I am also grateful for the technical support from Tony Fountaine of Ford Motor Company. It has been my pleasure and privileges to work with all of them.

Many aspects of my research projects have received financial support from Canada Research Chair Program, Canada Foundation of Innovation (CFI), Ontario Innovation Trust (OIT), Natural Sciences and Engineering Research Council of Canada (NSERC), Ford Motor Company of Canada, other non-disclosed OEMs, AUTO21 Network of Centres of Excellence and the University of Windsor.

Last but not least, I am indebted to my parents and my husband Chao for their love and supports.

Yuyu Tan

TABLE OF CONTENTS

	Page
ABSTRACT.....	iii
LIST OF PUBLICATIONS.....	iv
DEDICATION.....	v
ACKNOWLEDGEMENTS.....	vi
LIST OF TABLES.....	ix
LIST OF FIGURES.....	x
NOMENCLATURE.....	xiii
CHAPTER	
1 INTRODUCTION.....	1
1.1 Diesel Engine Combustion Control.....	1
1.2 Research Objectives.....	4
2 LITERATURE REVIEW.....	6
2.1 Combustion Energy Calculation.....	7
2.2 Heat Release Analysis.....	8
2.3 Diesel Injection System.....	9
2.3.1 Piezo Common-rail System.....	9
2.3.2 Operating Principle of the VCV and PCV.....	10
2.3.2.1 VCV Operating Principle.....	10
2.3.2.2 PCV Operating Principle.....	12
2.3.3 Rail-pressure Sensor.....	13
2.4 Solenoid Valve Control.....	14
2.5 PID Control Algorithm.....	15
3 PRELIMINARY EMPIRICAL AND MODELLING ANALYSIS.....	19
3.1 Empirical Analysis.....	19
3.2 Modelling Analysis.....	24
3.2.1 Heat Release Phasing and Duration Effects.....	24
3.2.2 Heat Release Shape Effects.....	31
3.2.3 Cylinder Pressure Characteristic Based Methods.....	33
3.2.4 Compression Ratio Effects.....	38

4	INDEPENDENT CONTROL OF EGR VALVE AND VCV, PCV	41
4.1	Design and Methodology	42
4.1.1	EGR Valve Control	44
4.1.2	VCV and PCV Control	47
4.2	Empirical Results and Discussions	51
4.2.1	EGR Valve Control Empirical Results and Analysis	51
4.2.2	Rail Pressure Control Empirical Results and Analysis	54
5	CONCLUSIONS AND RECOMMENDATIONS	56
	REFERENCES	59
	APPENDIX A DEVICE CONFIGURATIONS AND SPECIFICATIONS	63
	APPENDIX B DELPHI EGR VALVE SPECIFICATIONS	66
	APPENDIX C H-BRIDGE MOTOR DRIVER	67
	APPENDIX D VARIABLE COMPRESSION RATIO (VCR)	69
	APPENDIX E VARIABLE VALVE TIMING (VVT)	70
	APPENDIX F VARIABLE GEOMETRY TURBOCHARGER (VGT)	71
	VITA AUCTORIS	72

LIST OF TABLES

	Page
Table 3-1	Characteristics of the test engine20
Table 4-1	Two fuel metering approaches42
Table A-1	Specifications of NI PCI-6070E63
Table A-2	Specifications of NI cRIO-940163
Table A-3	Specifications of NI cRIO-920163
Table B-1	Specifications of Delphi EGR Valve [28]66
Table C-1	Specifications of Pololu High-Current Motor Driver Carrier [29]67

LIST OF FIGURES

	Page
Figure 1-1	1/ ϕ -T map showing regions of NO _x and soot formation [4]2
Figure 1-2	Research outline of the overall diesel engine control4
Figure 2-1	Typical modern diesel engine set-up with EGR, VVT, VGT control and turbocharger, after Dr. Ming Zheng [3]6
Figure 2-2	Definition of CA509
Figure 2-3	Common-rail injection system [13]10
Figure 2-4	Volume-control valve [14]11
Figure 2-5	Characteristic curve of VCV [14]11
Figure 2-6	Pressure-control valve [14]12
Figure 2-7	Characteristic curve of PCV [14]12
Figure 2-8	Characteristic curve of rail-pressure sensor [14]13
Figure 2-9	Empirical common-rail pressure fluctuation with injection event14
Figure 2-10	Solenoid structure15
Figure 2-11	PWM control signal15
Figure 2-12	PID control algorithm16
Figure 2-13	PID control response [16]18
Figure 3-1	University of Windsor Clean Diesel Engine Laboratory test cell19
Figure 3-2	Four-cylinder and single-cylinder mode empirical set-up, after Dr. Ming Zheng [4]20
Figure 3-3	Fuel mixing strategies implemented and tested at Clean Diesel Engine Laboratory [17]21
Figure 3-4	Diesel HCCI tests-effect of EGR on heat release phasing21
Figure 3-5	Diesel HCCI tests-effect of EGR on IMEP22
Figure 3-6	Comparison of diesel HTC and LTC heat release rates23
Figure 3-7	Comparison of diesel HTC and LTC η_{ind}23
Figure 3-8	Specified input conditions by varying the combustion phasing and duration24
Figure 3-9	Cylinder pressure for different heat release phasing25
Figure 3-10	Cumulative heat release for different heat release durations26
Figure 3-11	Cylinder pressure for different heat release durations26

Figure 3-12	p-V diagram showing heat release duration effects	27
Figure 3-13	Heat release duration effects on engine performances	27
Figure 3-14	Effect of CA50 and heat release duration on η_{ind}	28
Figure 3-15	Effect of CA50 and heat release duration on η_{ind} , p_{max} and $(dp/d\theta)_{max}$	29
Figure 3-16	Effect of CA50 on indicated power, heat transfer and exhaust energy	29
Figure 3-17	p-V diagram for early- and late-ignition combustion	30
Figure 3-18	Logarithmic p-V for the early- and late-ignition combustion	30
Figure 3-19	Specified input conditions with different heat release shapes	31
Figure 3-20	Effect of CA50 on η_{ind} for different heat release shapes with a fixed heat release duration	32
Figure 3-21	Map showing effect of CA50 and combustion duration on η_{ind} for different heat release shapes	33
Figure 3-22	The cylinder pressure traces characteristics [4]	34
Figure 3-23	The correlation between CA50 and $\theta_{p_{max}}$ for different heat release durations [4]	34
Figure 3-24	The rate-of-pressure-rise traces characteristics [4]	35
Figure 3-25	The correlation between CA50 and $\theta_{(dp/d\theta)_{max}}$ for different heat release durations [4]	36
Figure 3-26	The correlation between CA50 and p_{max} for complex and split heat release rates [4]	37
Figure 3-27	The correlation between CA50 and $\theta_{(dp/d\theta)_{max}}$ for complex and split heat release rates [4]	37
Figure 3-28	Cylinder pressure traces for different compression ratio	38
Figure 3-29	η_{ind} for different r_c and HR phasing and duration	39
Figure 3-30	Map showing effect of CA50 and compression ratio on η_{ind}	39
Figure 3-31	Map showing effect of CA50 and combustion duration on η_{ind} for compression ratios 15 and 17.8	40
Figure 4-1	Independent control of EGR valve and common-rail pressure	41
Figure 4-2	H-bridge circuit set-up in Clean Diesel Engine Laboratory	42
Figure 4-3	Empirical set-up of Delphi EGR valve in Clean Diesel Engine Laboratory (a), EGR valve terminals (b) and EVP scheme (c)	43
Figure 4-4	EGR valve position sensor response	43
Figure 4-5	PID control block diagram in LabVIEW	44
Figure 4-6	Empirical set-up of the Delphi EGR valve control	45
Figure 4-7	Detailed wire connection for Delphi EGR valve control	45

Figure 4-8	Algorithm flow chart of the Delphi EGR valve control program	46
Figure 4-9	Front panel and block diagram for Delphi EGR valve control program	46
Figure 4-10	Fast compensation control algorithm block diagram in LabVIEW	47
Figure 4-11	Schematic control set-up of the common-rail pressure control	48
Figure 4-12	The original OEM set-up for VCV control (left) and the independent VCV control set-up (right)	48
Figure 4-13	VCV control front panel (up) and block diagram (bottom)	49
Figure 4-14	The original OEM set-up for PCV control (left) and the independent PCV control set-up (right)	50
Figure 4-15	LabVIEW dialog window for selecting RT and FPGA target (left), project window (right)	50
Figure 4-16	FPGA front panel (left) and block diagram (right) for PCV control	51
Figure 4-17	RT front panel (left) and block diagram (right) for PCV control	51
Figure 4-18	Comparison between different control algorithms	52
Figure 4-19	Empirical results of PID control with SP variations	52
Figure 4-20	Empirical results of PID control under steady conditions	53
Figure 4-21	Empirical results of valve malfunction case	54
Figure 4-22	Soot accumulation on EGR valve (left), EGR valve after cleaning (right)	54
Figure 4-23	Duty cycle of PWM control current of VCV and PCV vs. injection pressure	55
Figure A-1	Channel configuration of NI cRIO-9401	64
Figure A-2	FPGA channel selection	65
Figure A-3	FPGA successful compile report	65
Figure C-1	H-bridge motor driver carrier [29]	67
Figure C-2	H-bridge circuit [29]	67
Figure D-1	VCR operating principles [30]	69
Figure E-1	VVT actuator [31]	70
Figure F-1	VGT vanes in exhaust flow [32]	71

NOMENCLATURE

AC	Alternating Current	[A]
AHRR	Apparent Heat Release Rate	
AI	Analog Input	
ATDC	After Top Dead Center	
abs	Absolute	
BTDC	Before Top Dead Center	
CA50	Crank Angle of 50% Heat Released	[°CA]
Comb.	Combustion	
Comp.	Compression	
CR	Common Rail	
cRIO	Compact Reconfigurable Input / Output Module	
D	Cylinder Diameter	[m]
D	Duty Cycle	[%]
DAQ	Data Acquisition	
DC	Direct Current	[A]
DCP	Diesel Common-rail Pump	
$(dp/d\theta)_{\max}$	Maximum Rate-of-pressure Rise	[bar/°CA]
e	Error	
E	Internal Energy	[J]
ECU	Engine Control Unit	
EGR	Exhaust Gas Recirculation	
EMF	Electro-Magnetic Force	[N]
eoc	End of Combustion	[°CA]
EOC	EGR Oxidation Catalyst	
EVP	Exhaust Valve Position Sensor	
FPGA	Field Programmable Gate Array	
GND	Ground	
HCCI	Homogenous Charge Compression Ignition	
HP	High-pressure	

HPP	High-pressure Pump	
HTC	High Temperature Combustion	
Hz	Hertz	
IMEP	Indicated Mean Effective Pressure	[bar]
I/O	Input/Output	
K_c	Controller Gain	[-]
T_i	Integral Time, Reset Time	[minutes]
T_D	Derivative Time, Rate Time	[minutes]
KS/s	Kilo Samples per Second	
L	Litre	
LTC	Low Temperature Combustion	
MS/s	Mega Samples per Second	
NI	National Instrument	
NO _x	Oxides of Nitrogen	
ns	Nano-second	
OEM	Original Equipment Manufacturer	
PCV	Pressure-control Valve	
PID	Proportional-Integral-Derivative	
p_{int}	Intake Pressure	[bar]
p_{max}	Maximum Cylinder Pressure	[bar]
PM	Particulate Matter	
PV	Process Variable	
PWM	Pulse Width Modulation	
Q	Cumulative Heat Release	[J]
r_c	Compression Ratio	[-]
Re	Reynolds Number	[-]
RP	Rail Pressure	[bar]
RPM	Revolutions Per Minute	[1/minute]
RT	Real-time	
SAES	Synthetic Atmosphere Engine Simulation	
soc	Start of Combustion	[°CA]
SOI	Start of Injection	[°CA]

SP	Set-point	
T	Working Fluid Temperature	[K]
T_{PWM}	Duration of the PWM Signal	[s]
TDC	Top Dead Center	
T_{int}	Intake Temperature	[K]
T_{ON}	On-time of the PWM Signal	[s]
TTL	Transistor-transistor Logic	
T_w	Cylinder Wall Temperature	[K]
VCR	Variable Compression Ratio	
VCV	Volume-control Valve	
VGT	Variable Geometry Turbocharger	
VI	Virtual Instrument	
VVT	Variable Valve Timing	
zero-D	Zero-Dimensional	
ϕ	Equivalence Ratio	[-]
θ, CA	Crank Angle	[°CA]
θ_{pmax}	Crank Angle of Maximum Cylinder Pressure	[°CA]
$\theta_{(dp/d\theta)max}$	Crank Angle of Maximum Rate-of-pressure Rise	[°CA]
μs	Microsecond	
ΔHR	Heat Release Duration, Combustion Duration	[°CA]
η_{ind}	Indicated Thermal Efficiency	[%]

CHAPTER I

1 INTRODUCTION

Electronic engine control has become a major research arena of technological innovation in the automotive industry over the last decades [1]. The immense new requirements for ultra clean in-cylinder combustion, sophisticated exhaust after-treatment, extended operational robustness, and higher fuel efficiency have propelled new developments in engine controls in order to improve the modern diesel engine performances. High-pressure fuel injection systems for diesel engines have been largely migrated from mechanical to electro-mechanical systems. New sensors and actuators have been developed, among them is the electronic feedback controlled exhaust gas recirculation (EGR) valve [2]. The precise and versatile control has improved modern diesel engines tremendously in traditionally weak aspects such as the noise and smoke. The new turbo-charged multiple-injection diesel engines are quiet, clean and having excellent torque characteristics while retaining their high energy efficiency. The latter has been critical to reduce the emissions of carbon dioxide (CO_2), a greenhouse gas.

1.1 Diesel Engine Combustion Control

Diesel engines have inherently high thermal efficiencies, resulting from their high compression ratio and fuel lean operation. However, high flame temperatures predominate because locally stoichiometric air-fuel ratios prevail in such heterogeneous combustion processes [3]. Therefore, diesel engine combustion generates a large amount of NO_x because of the high flame temperature in the presence of abundant oxygen and nitrogen, and a high level of soot because of the high non-homogeneity. The more recent work indicates that the low temperature combustion (LTC) in diesel engines is capable of reducing the soot and nitrogen oxides (NO_x) simultaneously [4]. This can be implemented by the heavy use of EGR together with the HCCI type of combustion. Diesel engines operating in HCCI mode tend to produce very low levels of NO_x and particulate matter (PM) [4]. However, at elevated engine loads, the flame temperature of

HCCI mode needs to be lowered with heavy EGR in order to retain the ultra-low NO_x and soot characteristics of HCCI.

The effects of in-cylinder temperature and air-fuel ratio on the formation of NO_x and soot can be illustrated in the ϕ -T, or $(1/\phi)$ -T, diagram in Figure 1-1. The burning of a diesel fuel in an excessively lean or rich homogeneous cylinder charge tends to release less heat than under stoichiometric burning and thus low temperature combustion prevails, the representative cases of which are the low-load lean HCCI ($\phi < 0.5$) and the fuel rich reforming ($\phi \approx 1.4 \sim 2$). The high-load HCCI and the smokeless combustion on the lean or rich side of stoichiometry are represented in the cases of “HCCI + EGR” in Figure 1-1 [4].

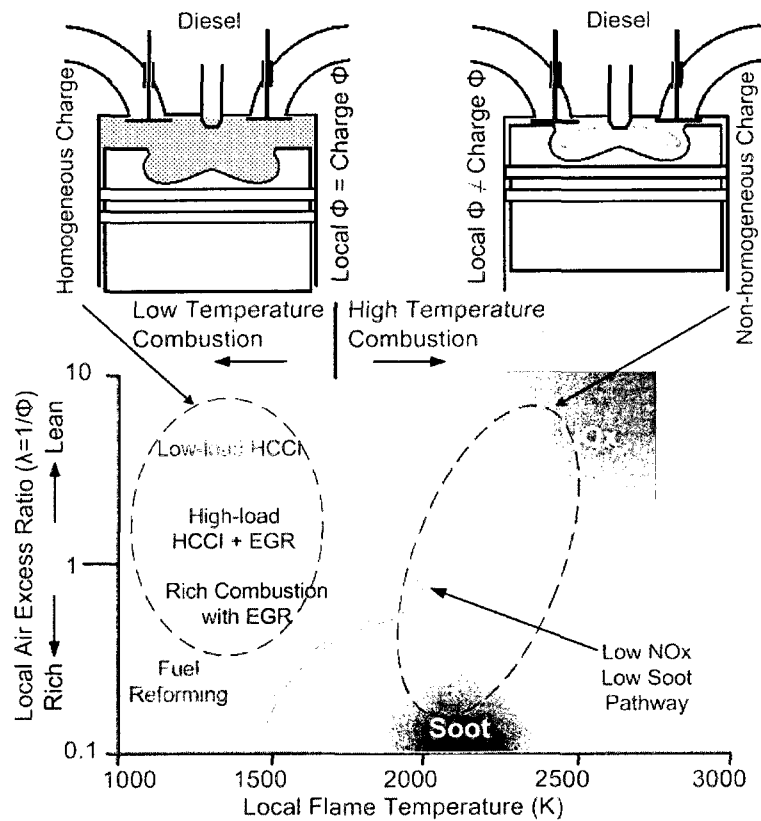


Figure 1-1: $1/\phi$ -T map showing regions of NO_x and soot formation [4]

In a reciprocating four-stroke multi-cylinder internal combustion engine, the transient air and exhaust flow rates and thus the pressures in the intake and exhaust manifolds fluctuate as the intake and exhaust valves open and close several times per cylinder per

second. This generates a pulsating unsteady pressure wave in the intake and exhaust system. This represents a major challenge for the accurate control of the EGR valve opening to compensate for the pressure wave effects in order to reach the required EGR ratio. The prompt and precise control of the EGR valve position, therefore, is essential for the determination of the amount of re-circulating exhaust gas.

To further improve the engine efficiency while maintaining ultra-low emissions, advanced engine technologies such as variable valve timing (VVT), variable compression ratio (VCR) and high-pressure piezo-electric injection, among others, are being implemented [5]. In addition, the volume-control and pressure-control electrical-mechanical valves (VCV and PCV) on the high-pressure fuel injection pump are used to control the fuel rail pressure. As a result, there is the need for increased computational capabilities that should achieve the precise control of the respective parameters.

Modern diesel engines commonly have engine control units (ECUs) that govern the rail pressure, EGR ratio, injection events, and *etc.* Specifically, the ECU normally is capable of determining the rail-pressure based on the engine operating condition in order to optimize the efficiency and power output. Concurrently, the ECU decides the required amount of EGR ratio and commands the EGR valve opening to lower the NO_x emission.

In order to control the rail pressure and EGR valve opening independently under laboratory conditions, substitution devises need to be developed with custom feedback algorithms and/or circuits. This is necessary because the ECU, which normally follows a strict engine look-up table to control the preset parameters, has to be deluded to allow for independent subsystem control.

The aim of this research is to develop and to apply diesel engine control strategies in order to fulfill the emission, cylinder pressure, and engine efficiency requirements. At the first stage of the control concepts development, basic analysis needs to be carried out. Computer modeling, such as engine cycle simulation, is considered as an efficient tool to analyze the independent effects of each operating or configuration parameters of the engine. Such modeling analysis can provide valuable insights for the advanced engine control.

1.2 Research Objectives

This research is aimed at providing preliminary empirical and theoretical preparations to facilitate the overall model-based diesel engine control work at the Clean Diesel Engine Laboratory, which is outlined in Figure 1-2 and this thesis work is highlighted.

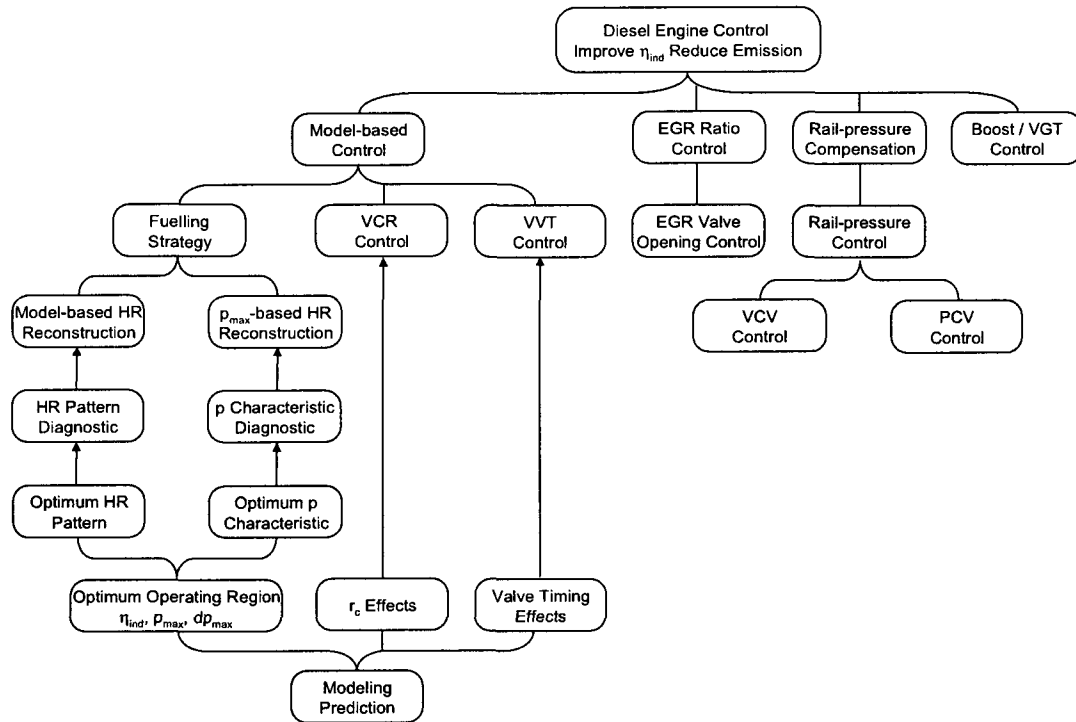


Figure 1-2: Research outline of the overall diesel engine control

As shown in Figure 1-2, in the present investigation the impact of heat-release patterns on the fuel efficiency is to be analyzed with zero-D engine cycle simulations. Preliminary work has been made to correlate the maximum cylinder pressure and maximum cylinder pressure-rise-rate with the combustion phasing and duration. Attempts have been made to identify the optimum efficiency at selected engine operating conditions. Overall, this thesis provides the modeling and empirical preparation that targets to improve diesel combustion in the following areas:

- To identify the major engine fuelling parameters that affect the thermal efficiency of the diesel engine cycle to facilitate model based control.

- To characterize the correlations between the cylinder pressure and the heat release pattern in order to develop cylinder pressure-based adaptive fuel-injection control strategies that will be used to stabilize the engine operation during the low-temperature combustion modes.
- To implement fuel injection control based on the operating ranges from the modeling analyses.

In the empirical preparation part of this thesis, independent high-precision controls on the fuel pressure of the diesel common-rail system and the EGR valve opening are to be accomplished by devising control algorithms that substitute the control from the ECU. A variety of control algorithms including manual control, fast feedback control and proportional integral and derivative (PID) control are to be implemented and tested to improve the response and precision of the EGR valve and the rail pressure control. This aspect of the research targets to explore and investigate a variety of control algorithms to achieve independent control in order to apply customized injection and combustion control strategies.

CHAPTER II

2 LITERATURE REVIEW

Modern diesel engines commonly involve sophisticated controls on the boost, EGR, and multi-event fuel injection [4,17,22], as shown in Figure 2-1. However, the engine system largely works in an overall open-loop strategy. The system works very well in the traditional high temperature combustion modes [6]. However, when the engine operates in low temperature combustion regions, the system operates less robust and a closed loop control strategy becomes necessary [4]. In order to establish such a close-loop system, modeling analysis and model-based control strategies for each of the sub-systems need to be established. Under such circumstances, it is considered that a zero-D model would be suitable to describe the in-cylinder combustion process [5,8].

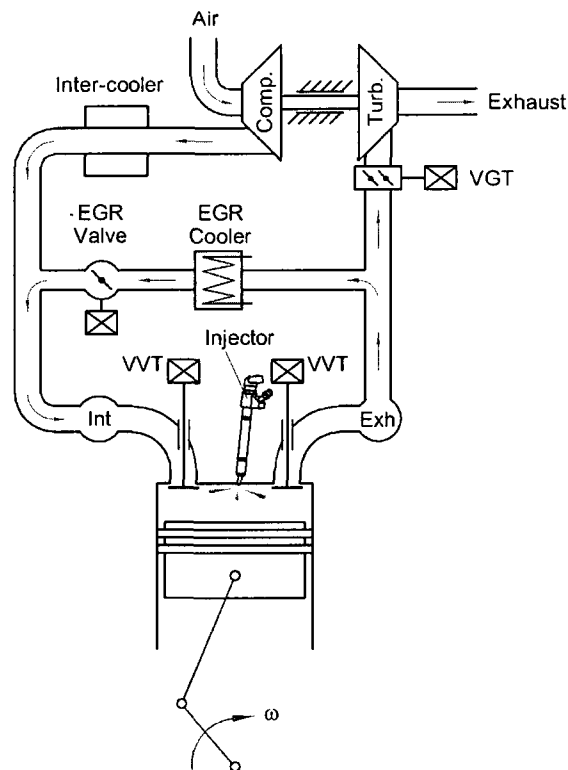


Figure 2-1: Typical modern diesel engine set-up with EGR, VVT, VGT control and turbocharger, after Dr. Ming Zheng [3]

2.1 Combustion Energy Calculation

In order to facilitate the diesel engine control work, a zero-D phenomenological engine cycle simulation program - Synthetic Atmosphere Engine Simulation (SAES) [7] – is adapted to analyze the energy release of the combustion process. [7]. This program was developed by Dr. Ming Zheng and Dr. Graham T. Reader. The model can generate cylinder pressure, temperature, heat release traces, and other operating parameters.

When both of the intake and exhaust valves are closed, the first law of thermodynamics in time step dt is applied to describe the cylinder working fluid under specified assumptions [7,8]:

$$dE = \delta Q + dM_f \cdot q_{vs} - dW = (E(T_2) - E(T_s)) - (E(T_1) - E(T_s)) \quad (2.1)$$

where, dE is the change in the internal energy, δQ is the heat transferred to or from the cylinder walls; dW is the work due to the piston motion; q_{vs} is the lower calorific value; M_f is the total amount of fuel injected; and dM_f is the fuel burnt in the time step. Additionally, T_1 , T_2 , and T_s are the temperatures at time steps t_1 and t_2 , and the reference condition respectively. The $(E(T_2) - E(T_s))$ and $(E(T_1) - E(T_s))$ terms represent the internal energy terms at states 2 and 1 measured above the reference temperature T_s .

The heat transfer δQ using the Annand's model [5,7,8] is described by the following equation.

$$\frac{\delta Q}{dt} = \frac{ak}{D} (\text{Re})^b (T - T_w) + c(T^4 - T_w^4) \quad (2.2)$$

where, a , b and c are empirical coefficients, k is the thermal conductivity, D is the cylinder diameter, Re is the Reynolds number, T is the working fluid temperature and T_w is the cylinder wall temperature.

The work term dW is, as in the ideal cycle, evaluated from the mean cylinder pressure:

$$dW = \left(\frac{P_1 + P_2}{2} \right) (V_2 - V_1) \quad (2.3)$$

The term $dM_f \cdot q_{VS}$ is the heat release term. A number of heat release models have been adapted in this research. The Wiebe heat release model, also known as the Wiebe function, has been used [7,8]. The fraction of fuel burnt, F_B , is described by:

$$F_B = 1.0 - \exp(-\delta_1 \tau^{\delta_2}) \quad (2.4)$$

$$\tau = \frac{\theta - \theta_i}{\theta_e - \theta_i} \quad (2.5)$$

where, δ_1 and δ_2 are empirical coefficients, τ is the combustion period, θ_i and θ_e are the crank angle of start of combustion (soc) and end of combustion (eoc) respectively, and θ is the current crank angle.

The heat release rate is derived by differentiating equation (2.4):

$$f_B = \frac{dF_B}{d\tau} = \delta_1 \delta_2 \tau^{(\delta_2-1)} \exp(-\delta_1 \tau^{\delta_2}) \quad (2.6)$$

The shape of the heat release curve is determined by the coefficients δ_1 and δ_2 . The phasing and duration of the heat release curve is controlled by θ_i and $(\theta_e - \theta_i)$.

2.2 Heat Release Analysis

A variety of engine control functions could be implemented and improved using heat release analysis. Heat release analysis is based on cylinder pressure data to analyze the combustion phasing that has been applied widely by other researchers. Besides the thermodynamic model, the SAES program also includes a heat-release model. In this research, the crank angle of 50% heat release (CA50) is defined as the crank angle at which the cumulative heat release reaches 0.5 as shown in Figure 2-2. The heat release phasing is defined as the variation of the CA50. The CA50 is commonly used for real-time close-loop control by other researchers [9-11].

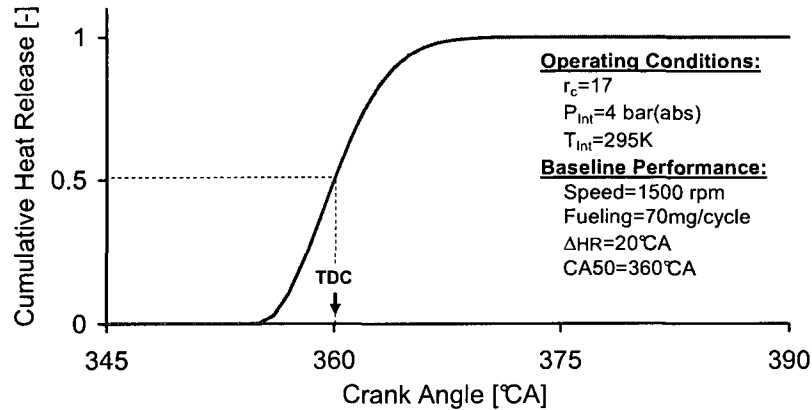


Figure 2-2: Definition of CA50

Soylu, [5] analyzed the effects of SOC, heat release duration, compression ratio and boost effects on natural gas HCCI combustion with a zero-D thermodynamic model. Wiebe heat release function and Annand's heat transfer correlation were used in his simulation. Bengtsson, and *et al.*, [9] proposed a method of estimating CA50 from maximum cylinder pressure (p_{max}). The estimation was based on the assumption that the crank angle of the maximum cylinder pressure (θ_{pmax}) is at the middle of the combustion (CA50). Hampson, [10] concluded that the maximum efficiency occurs when the centroid of the pressure rise at TDC and the increasing IMEP is accomplished by increasing the burn duration.

2.3 Diesel Injection System

2.3.1 Piezo Common-rail System

The Piezo common-rail system shown in Figure 2-3 mainly consists of a diesel common-rail pump (DCP), a high-pressure fuel rail, and Piezo controlled injectors. The high-pressure fuel rail which maintains the fuel at high pressure also acts as a fuel distributor and dampens pressure fluctuations caused by the fuel pulses delivered by the pump and the fuel injection cycles [12]. The diesel common-rail pump contains the internal transfer pump (ITP), the volume-control valve (VCV), the pressure-control valve (PCV), and the high pressure pump (HPP).

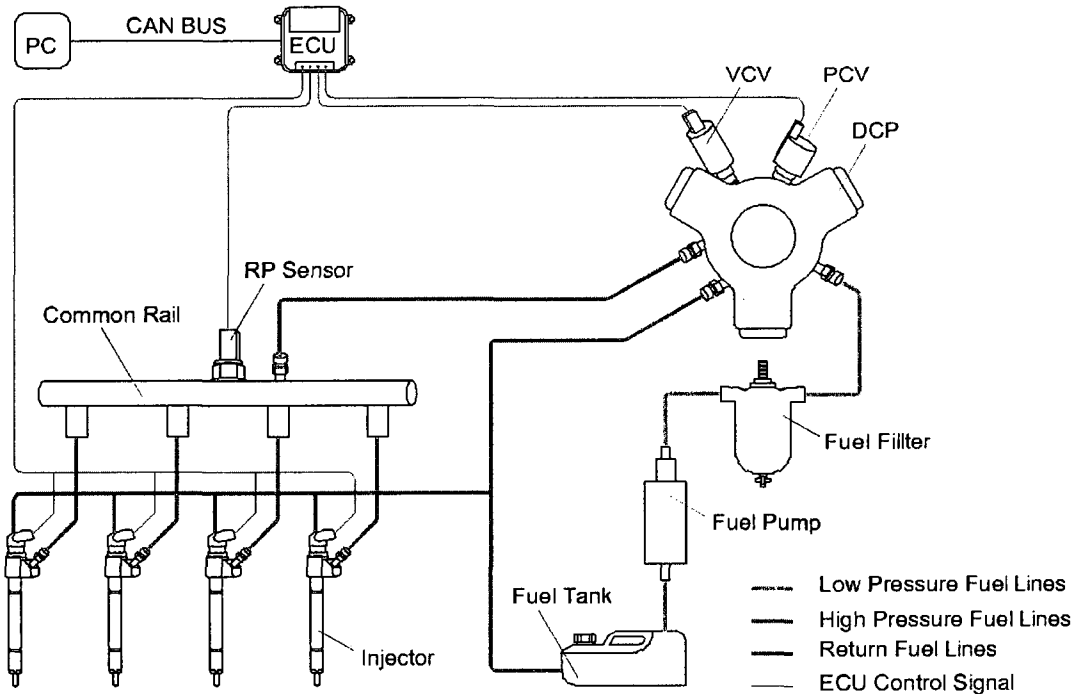


Figure 2-3: Common-rail injection system [13]

2.3.2 Operating Principle of the VCV and PCV

2.3.2.1 VCV Operating Principle

The VCV governs the amount of fuel drawn from the fuel tank by the internal transfer pump and then supplies the fuel to the high pressure pump. The high pressure pump delivers the high pressurized fuel to the fuel rail [14]. The operating principle of a typical VCV is illustrated in Figure 2-4. If there is no control current applied on the VCV, the valve closes by means of the force generated by the spring. The fuel delivery to the high pressure pump is interrupted. If commanded injection pressure set-point value increases, the VCV opens so that more fuel is delivered to the high pressure pump. The electromagnetic force (EMF) proportional to the control current works against the force of the spring. The opening of the VCV and thus the fuel supply amount is a function of the control current as shown in Figure 2-5.

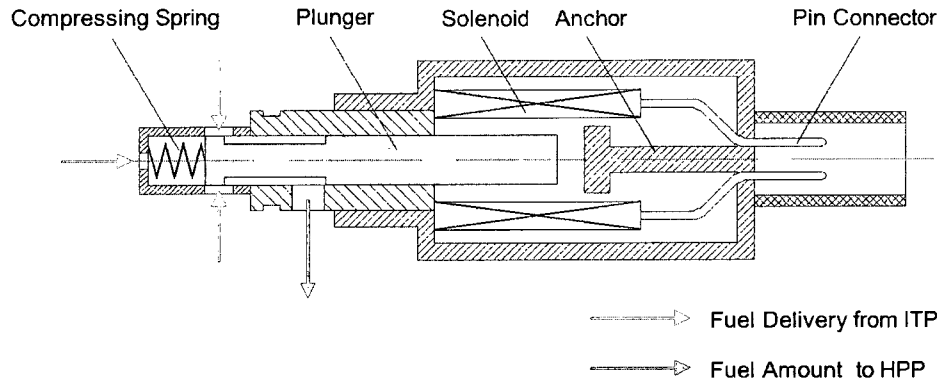


Figure 2-4: Volume-control valve [14]

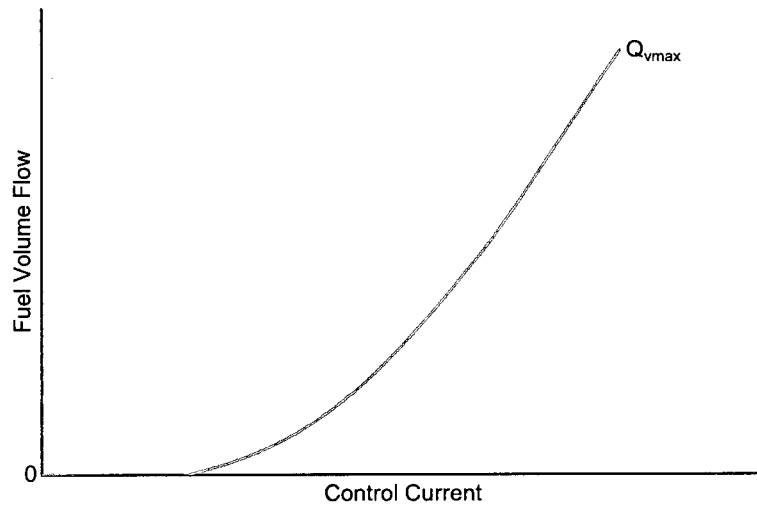


Figure 2-5: Characteristic curve of VCV [14]

The EMF works against the force of the spring can be represented by the following equation:

$$EMF = -F_s = -K \cdot |\Delta x - x_0| \quad (2.7)$$

where, the EMF is the electro-magnetic force, F_s is the spring force, K is the spring constant, Δx is the compression distance of the spring, x_0 is the distance that the spring has to be compressed before opening the VCV.

2.3.2.2 PCV Operating Principle

The operating principle of a typical PCV is illustrated in Figure 2-6. The PCV regulates the pressure in the common-rail as a factor of engine load [12]. If the pressure in the fuel rail is too high, the PCV opens so that excess fuel escapes from the fuel rail and returns to the fuel tank. If the pressure in the fuel rail is too low, the PCV closes until a state of equilibrium is reached between the high fuel pressure and the combined force of the electro-magnet and the spring [12,14]. The electro-magnet force and thus the common-rail pressure are proportional to the control current. As shown in Figure 2-7, the rail pressure and the control current follow linear relationship within the operating range.

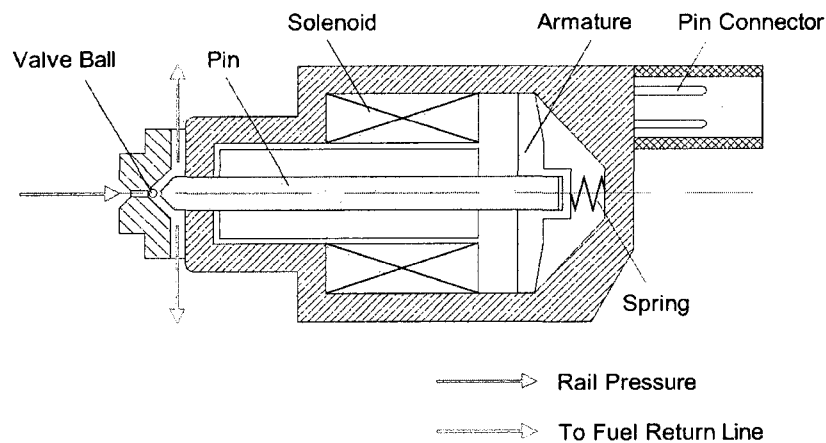


Figure 2-6: Pressure-control valve [14]

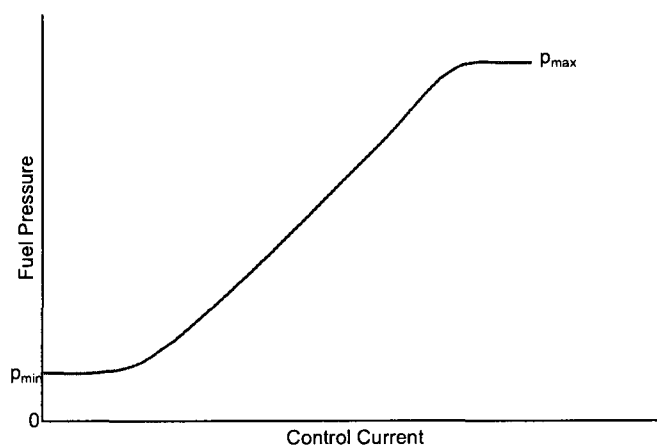


Figure 2-7: Characteristic curve of PCV [14]

The force equilibrium of the PCV operating can be defined as:

$$F_{RP} = EMF + F_s \quad (2.8)$$

where, the F_{RP} is the force of the rail pressure acting on the valve ball illustrated in Figure 2-6.

2.3.3 Rail-pressure Sensor

The rail-pressure sensor measures the fuel pressure in the high-pressure fuel rail. The pressure value is converted into the electric potential signal and is used for the computation of the pressure regulation through the PCV [14]. The characteristic curve of rail-pressure sensor is displayed in Figure 2-8. The rail pressure sensor voltage output is linearly correlated to the rail pressure value.

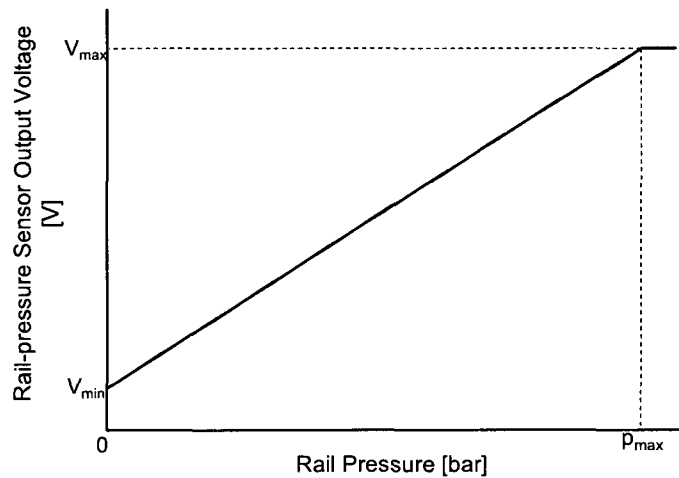


Figure 2-8: Characteristic curve of rail-pressure sensor [14]

A cylinder pressure curve by converting the rail-pressure voltage signal obtained from the rail-pressure sensor during an engine test in Clean Diesel Engine Laboratory into bars is shown in Figure 2-9. Rail-pressure fluctuations caused by the fuel injection event are noticeable in this figure. This fluctuated fuel pressure wave will affect the later injection events since the uncertainty that the later injection events are conducted during the decreasing or increasing of the common-rail pressure exists. If the fuel is injected when

the rail-pressure decrease, the actual fuel injection quantity will be less than the commanded value. Therefore, the actual fuel injection quantity is not guaranteed. The compensation of the common-rail pressure wave is necessary in order to perform accurate fuel injection control. The independent control of VCV and PCV in this thesis work is a preparation for the common-rail pressure wave compensation strategy development.

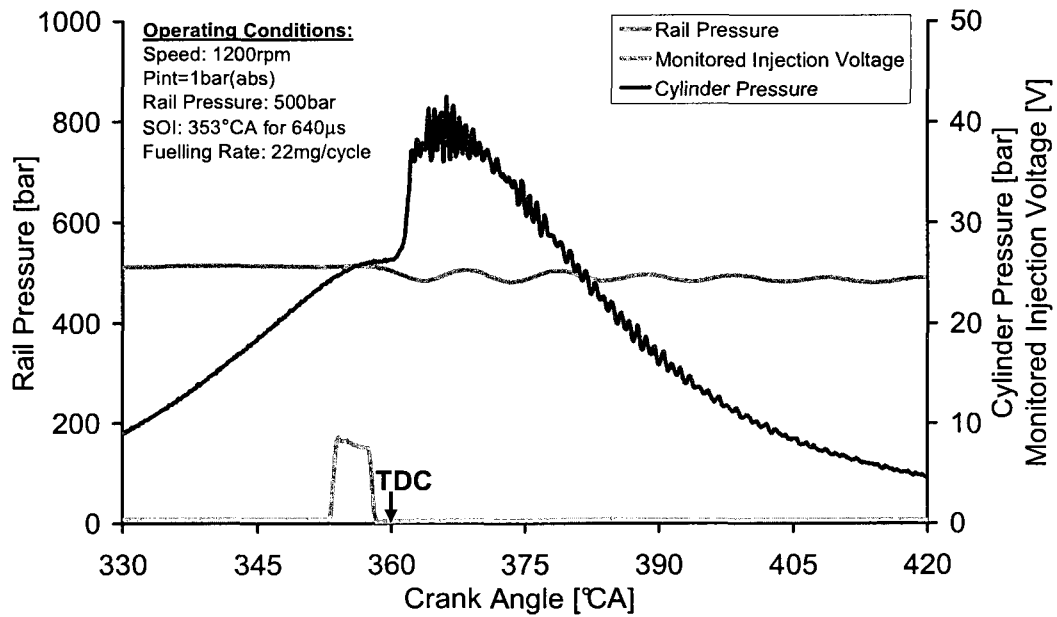


Figure 2-9: Empirical common-rail pressure fluctuation with injection event

2.4 Solenoid Valve Control

The EGR valve, the VCV and the PCV are electric solenoid actuated valves. Solenoids are normally built by winding a coil of wire around a moveable soft iron plunger as illustrated in Figure 2-10. The solenoid converts the electrical power into mechanical linear movements against the return spring and the hydraulic or pneumatic forces. A linear stroke of a solenoid valve typically has relatively short mechanical movement. For instance, the full stroke of the tested EGR valve is 28 mm, while the full stroke of a PCV is typically less than 1~2 mm.

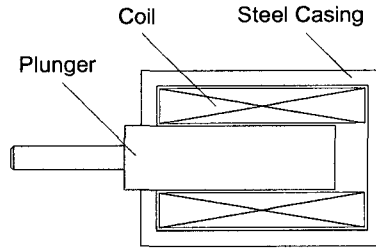


Figure 2-10: Solenoid structure

When the electric current passes through the coil, the plunger moves to close the magnetic loop. The driving current can be direct current (DC), alternating current (AC), or pulse width modulated (PWM) current. If the DC is applied as the driven current, the solenoid will burn-out because of its low coil resistance. PWM drive signal is the best for solenoids to avoid over-heating and burn-out because the coil inductance restricts the coil current within limited value. A typical PWM control signal is illustrated in Figure 2-11.

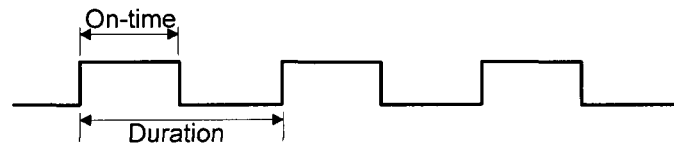


Figure 2-11: PWM control signal

The duty cycle of the PWM signal is defined by the following equation.

$$D\% = \frac{T_{ON}}{T_{PWM}} \cdot 100\% \quad (2.9)$$

where, T_{ON} is the on-time, and T_{PWM} is the duration of the PWM signal. The control of the valve open extent is realized by adjusting the duty cycle of the PWM signal.

2.5 PID Control Algorithm

The proportional-integral-derivative (PID) controller is a widely-used feedback control algorithm which involves three individual parameters: the proportional, the integral and derivative terms [15]. As shown in Figure 2-12, the PID controller eliminates the error

between a measured process variable (PV) and a desired set-point (SP) based on a weighted sum of the three terms.

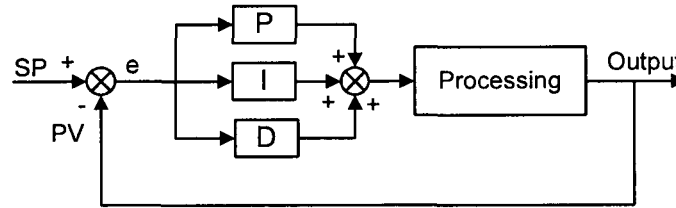


Figure 2-12: PID control algorithm

The error, e , is the difference between the measured and set values:

$$e = SP - PV \quad (2.10)$$

where, the SP is the set-point value, and the PV is the process value.

The PID control behaviors are described mathematically in the following equations.

$$u_p(t) = K_C \cdot e \quad (2.11)$$

$$u_I(t) = \frac{K_C}{T_I} \cdot \int_0^t e \cdot dt \quad (2.12)$$

$$u_D(t) = K_C \cdot T_D \frac{de}{dt} \quad (2.13)$$

where, K_C is the controller gain, T_I is the integral time (reset time) in minutes, T_D is the derivative time (rate time) in minutes, and $u_p(t)$, $u_I(t)$ and $u_D(t)$ are proportional, integral and derivative action respectively.

Controller output is the summation of the proportional, integral, and derivative term.

$$u(t) = u_p(t) + u_I(t) + u_D(t) \quad (2.14)$$

Thus, the practical PID controller is expressed in the following equation [15].

$$u(t) = K_c \left(e + \frac{1}{T_i} \int_0^t e \cdot dt + T_d \frac{de}{dt} \right) \quad (2.15)$$

The proportional term reduces the current measured error value. The larger the proportional parameter, the faster the system reacts to eliminate the error. However, overshoot happens and thus system stabilization reduces if the proportion parameter is too large.

The integral term is proportional to the accumulated offset over time that should have been corrected previously. The smaller the integral time, the greater the contribution comes from the integral term. The integral term increases system instability because of its response to the previous error even when the set-point is reached.

The derivative term predicts the rate of the error change. Derivative control reduces the magnitude of the overshoot. However, because the differentiation of a signal amplifies the noise levels, the derivative term is highly sensitive to noise in the measured signal and causes system instability.

By tuning the three parameters of the PID controller, the control requirement including response time, overshoot and oscillation can be fulfilled. The tuning process follows the sequence of proportional, integral and derivative. First step is to increase the proportional parameter until the fast response, small overshoot are obtained. Second step is to reduce the proportional parameter to 50~80% and set the integral time to a larger value. Then the consequent steps are to decrease the integral time while adjust the proportional parameter accordingly until the response PV is satisfied. The last step is to increase the derivative time from zero and adjust the proportional parameter and integral time for better and faster response.

Figure 2-13 demonstrates the effects of a PID controller with different P or I actions. The set-point is 40. The proper tuned response is plotted in red line [16].

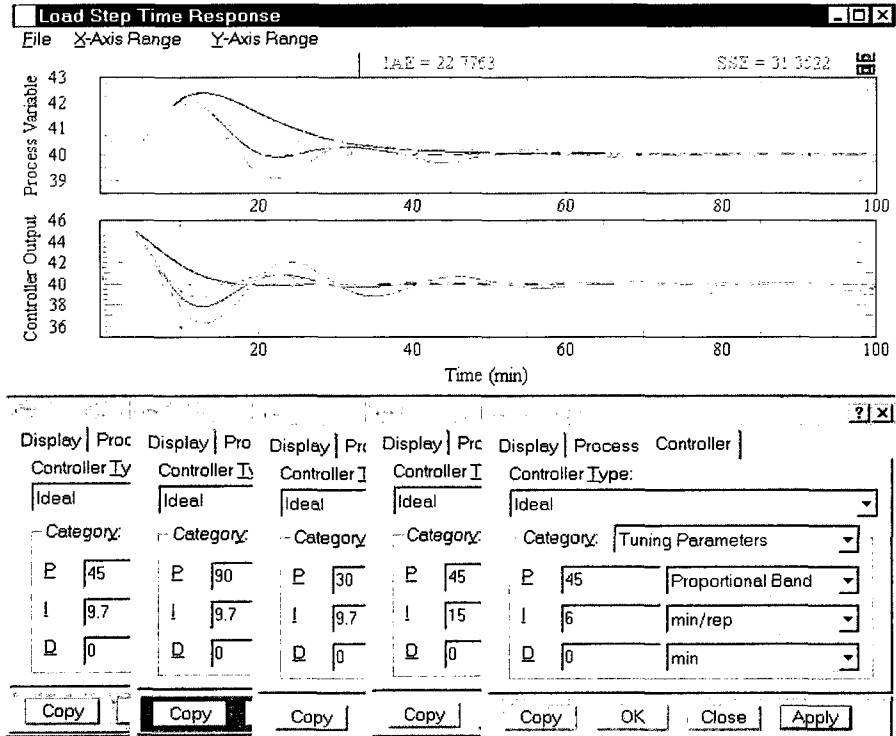


Figure 2-13: PID control response [16]

The PID is the most common control technique in the industry [15]. The control applications can be realized by utilizing the PID control software toolkit from National Instruments. Nevertheless, it should be noted that the general nature of PID control does not guarantee optimal control of the system.

CHAPTER III

3 PRELIMINARY EMPIRICAL AND MODELLING ANALYSIS

A reliable feedback signal is the precondition of the real-time adaptive control. In this chapter, a control-oriented preliminary empirical and modeling analysis has been carried out. Major engine operating parameters that includes the phasing, duration and shaping of the heat release, and compression ratio effects on engine performance are evaluated. The feasibility of the feedback signal for the adaptive control is discussed.

3.1 Empirical Analysis

The research platform is based on a 4-cylinder Ford common-rail diesel engine detailed in Figure 3-1 and Table 3-1 [17]. This engine has been configured and instrumented to operate on a single cylinder (0.5L) mode as shown in Figure 3-2 [19]. Laboratory researchers Raj Kumar and Xiaoye Han and *et al.* [19] have made major contributions to set up the system. All the empirical studies in this thesis have been conducted under independently controlled levels of EGR, intake boost, and exhaust backpressure, when the engine is fueled with a conventional diesel fuel for running in the single cylinder mode.



Figure 3-1: University of Windsor Clean Diesel Engine Laboratory test cell

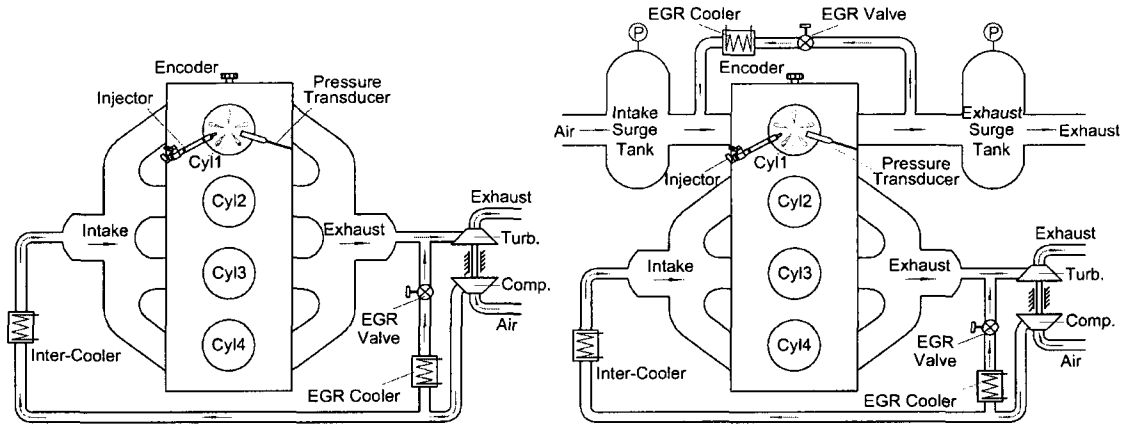


Figure 3-2: Four-cylinder and single-cylinder mode empirical set-up, after Dr. Ming Zheng [4]

Table 3-1: Characteristics of the test engine

Engine Type	4 Cylinder, 4 Stroke Ford DuraTorq “Puma”
Displacement [cm³]	1998
Bore [mm]	86
Stroke [mm]	86
Compression Ratio	18.2:1
Combustion System	Direct Injection
Injection System	DELPHI Common-rail (up to RP≈1600bar)

The volatility of diesel fuels is much lower than that of gasoline fuels. This explains the implementation challenge to form a cylinder charge of high homogeneity with diesel fuels. In order to achieve the homogeneous cylinder charge with diesel fuels, a variety of fuel delivery strategies have been developed in Clean Diesel Engine Laboratory as outlined in Figure 3-3 [17,22]. In many cases, combined uses of the techniques are involved in achieving the best emission reduction and high fuel efficiency.

Previous empirical results have indicated that the engine emission and fuel efficiency can be optimized by adopting the appropriate combustion phasing [4,17,21,22]. The use of EGR has been determined experimentally as the most effective way among the combustion phasing modulation techniques that include the control of fuel injection scheduling and pressure, boost, and intake temperature [20].

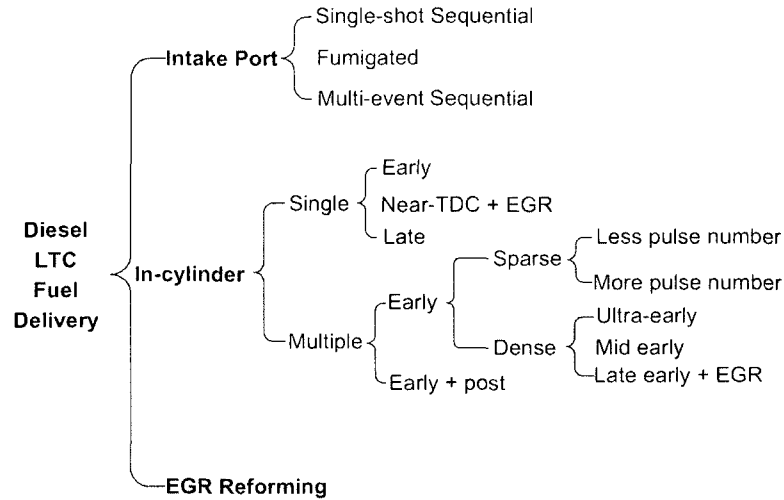


Figure 3-3: Fuel mixing strategies implemented and tested at Clean Diesel Engine Laboratory [17]

To investigate the EGR effect, the fuelling rate is kept constant during the tests shown in Figure 3-4 and Figure 3-5. With the increasing of EGR ratio from 41% to 60%, the heat release phasing has been postponed from 349°CA to 360°CA, as shown in Figure 3-4.

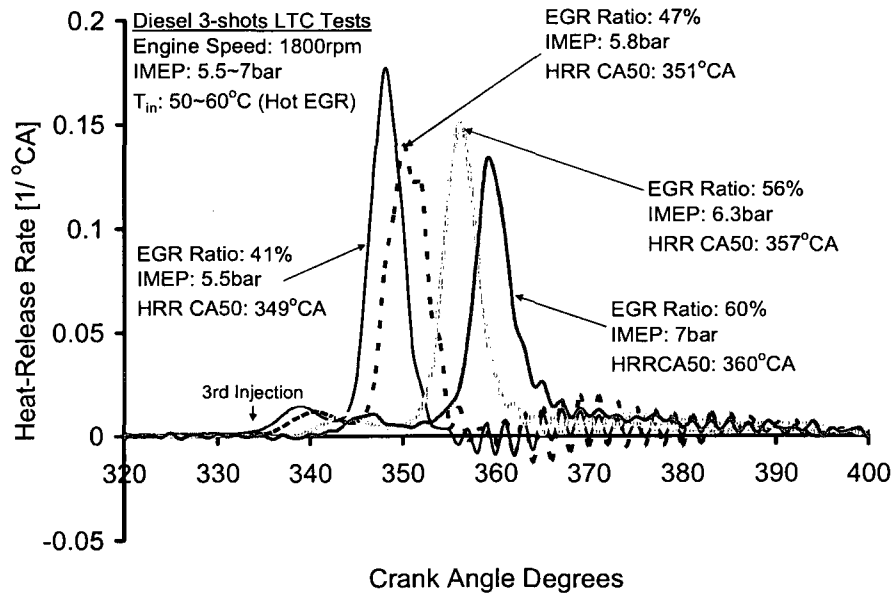


Figure 3-4: Diesel HCCI tests-effect of EGR on heat release phasing

Figure 3-5 demonstrates that the resultant indicated mean effective pressure (IMEP) increases with the EGR ratio increases. The reason for that is the combustion phasing, indicated by the CA50 is postponed towards the piston top dead centre (TDC) as the increasing of the EGR ratio. The highest IMEP is observed when the CA50 is approaching the TDC.

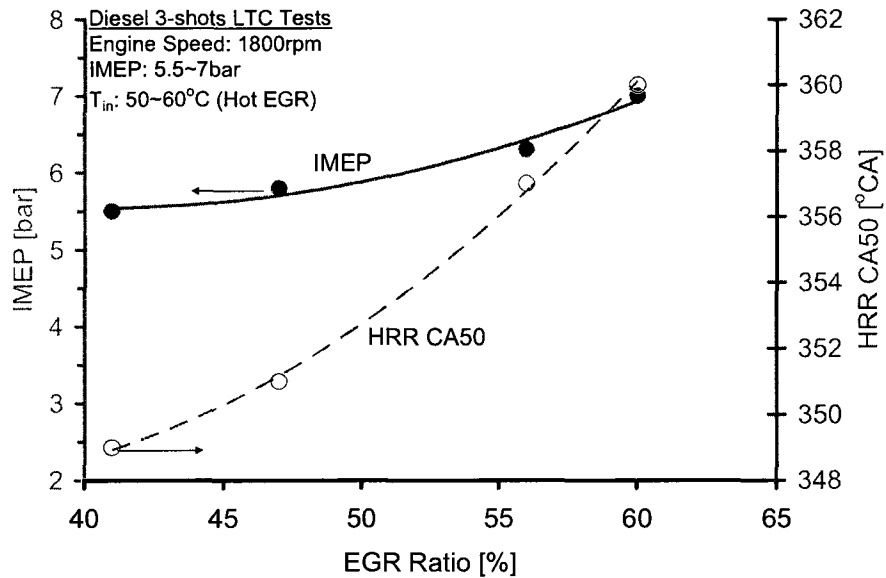


Figure 3-5: Diesel HCCI tests-effect of EGR on IMEP

To further investigate the EGR effects, the IMEP is kept constant as the CA50 shifts with the EGR ratio. For the HCCI test results in Figure 3-6 and Figure 3-7, an improvement in the indicated thermal efficiency (η_{ind}) is also observed as the CA50 approaches the TDC. Nevertheless, compared with the conventional diesel HTC case, the diesel HCCI cycle (a LTC case) efficiencies are generally lower or at most compatible, which is in agreement with the more recent reports from other researchers [24,25].

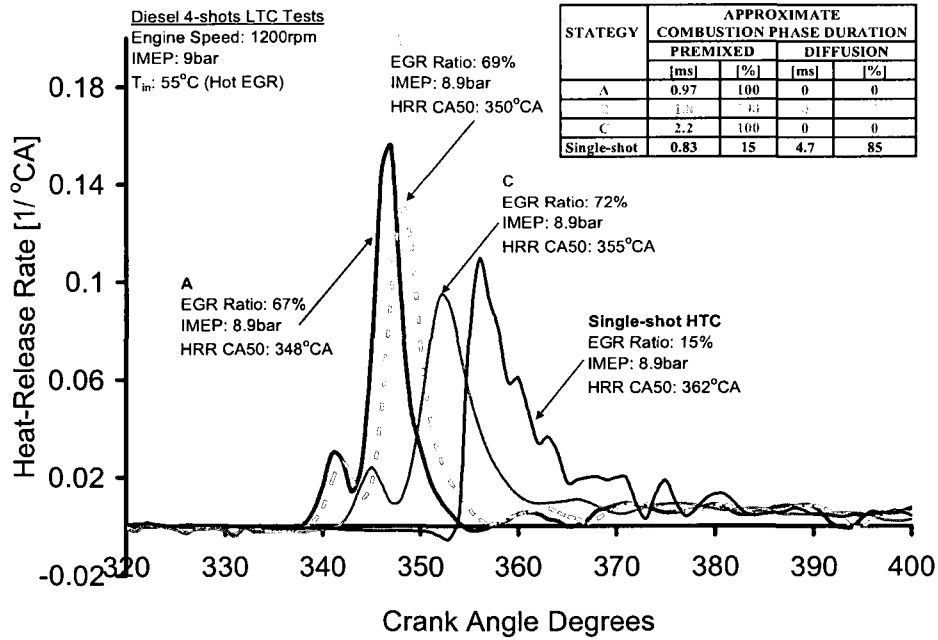


Figure 3-6: Comparison of diesel HTC and LTC heat release rates

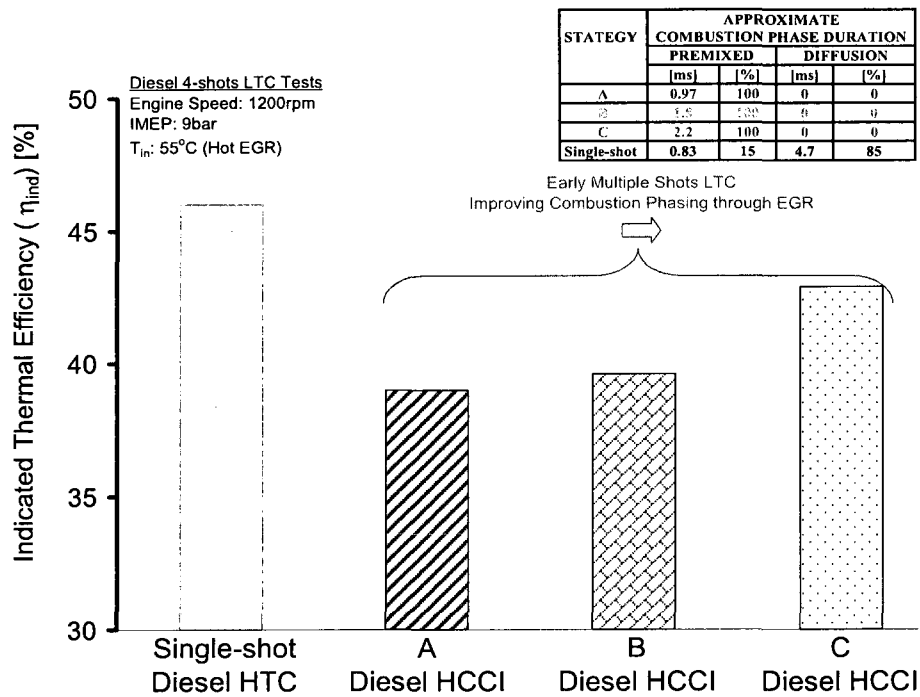


Figure 3-7: Comparison of diesel HTC and LTC η_{ind}

3.2 Modelling Analysis

As demonstrated in the empirical analysis section, the heat release phasing by means of EGR ratio modulation can be treated as a significant factor in improving the engine performance. In this section, the impact of heat release phasing, duration, and shaping on fuel efficiency has been analyzed with the SAES program. The simulation results provide further insights for the identification of the optimum heat release patterns in order to facilitate the heat release based feedback control. In addition, the effects of compression ratio are also investigated. Preliminary analysis for adaptive control based on cylinder pressure characteristic has been discussed in section 3.2.3.

3.2.1 Heat Release Phasing and Duration Effects

Diesel engines typically have higher combustion efficiency than gasoline engines [18]. In order to target the first principles of combustion control, complete combustion is assumed (100% fuel to heat energy conversion) in the model analyses. The simulation was performed by varying the timing and duration of the heat release curves, as demonstrated in Figure 3-8. The impacts on cylinder pressure and engine performance are discussed accordingly.

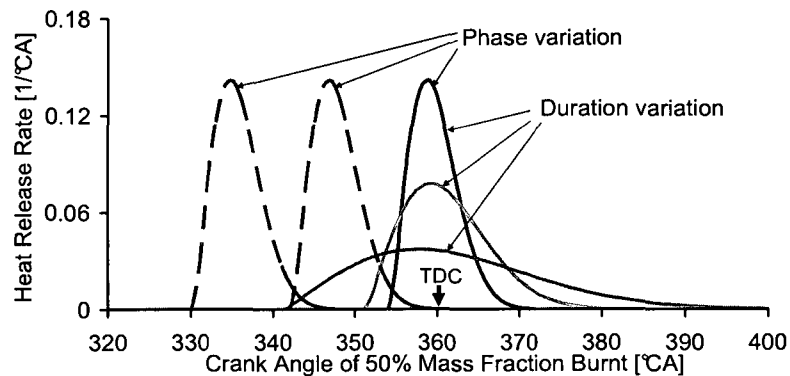


Figure 3-8: Specified input conditions by varying the combustion phasing and duration

In the simulation, it is set that the engine has the compression ratio of 17:1 running at 1500rpm with the intake pressure of 4 bar (abs). The fueling rate is kept at 70mg per cycle.

Firstly, the heat release phasing effects is examined by varying the CA50 from 340 to 420°CA with fixed heat release duration of 20°CA. The cylinder pressure and heat release curves are shown in Figure 3-9. The maximum cylinder pressure is very high (> 300 bar) when the CA50 is slightly before or at TDC. The maximum cylinder pressure is very sensitive to the phasing change. Delaying the heat release phasing from 340 to 380°CA reduces peak pressure by approximately 58%.

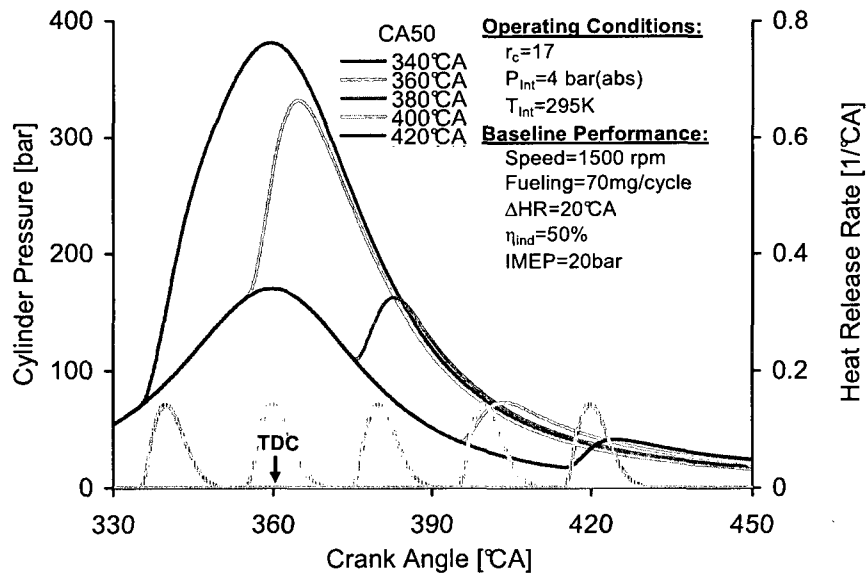


Figure 3-9: Cylinder pressure for different heat release phasing

Secondly, under the same operating conditions, the simulation of the heat release duration effects, which corresponds to the apparent burning duration in actual engine tests, is carried out by fixing the combustion timing represented by the position of CA50. The cumulative heat release curves cross at point (360°CA, 0.5), indicating the CA50 is fixed at 360°CA in Figure 3-10. The simulated heat release duration varies from 5 to 80°CA. Per unit area under the heat release rate curve, a shorter heat release duration represents a faster (narrower area) combustion process while a longer heat release duration represents a slower (wider area) combustion process.

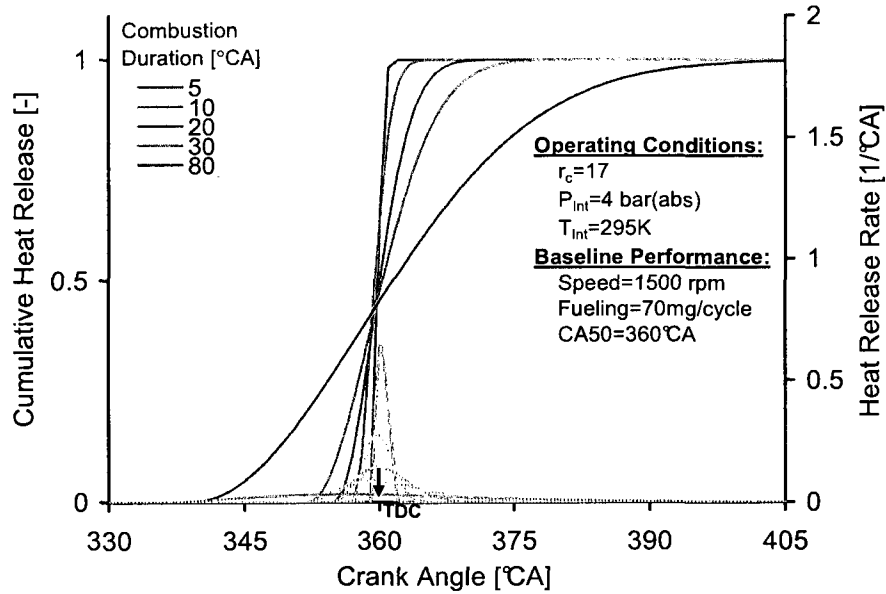


Figure 3-10: Cumulative heat release for different heat release durations

From Figure 3-11, the variation in heat release duration has significant effect on cylinder pressure when the CA50 is at 360°CA. As the duration increases from 5 to 80°CA, the maximum cylinder pressure decreases by 70 bar (20%).

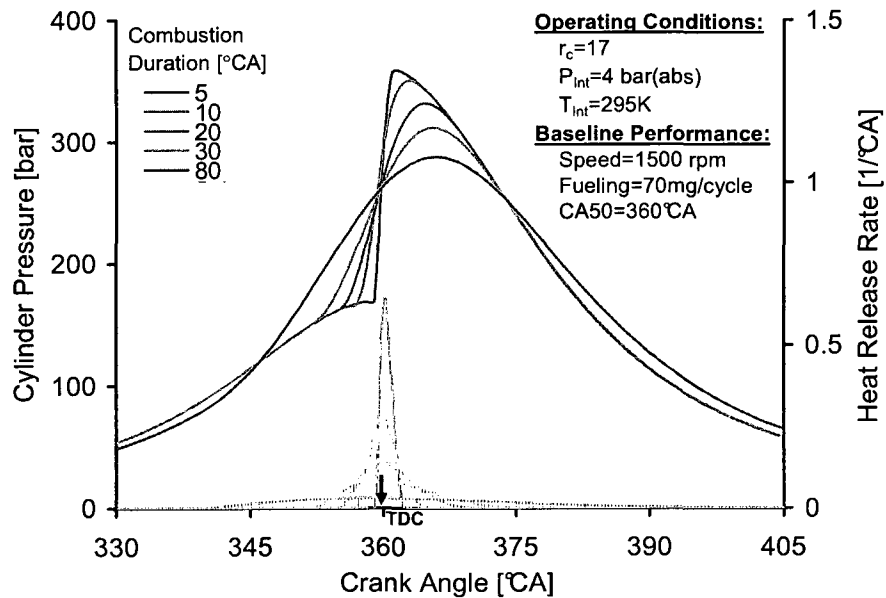


Figure 3-11: Cylinder pressure for different heat release durations

Heat release duration has insignificant effect on the engine performance. The comparison of p-V diagram for heat release duration of 5°CA and 40°CA is shown in Figure 3-12. Area enveloped in the p-V diagram and thus the IMEP is smaller for the longer heat release duration. When the CA50 is placed at TDC (360°CA) and the duration of the heat release is less than 80°CA, both the indicated thermal efficiency and the IMEP decrease only slightly as the heat release duration increases from 5 to 80°CA, as indicated in Figure 3-13.

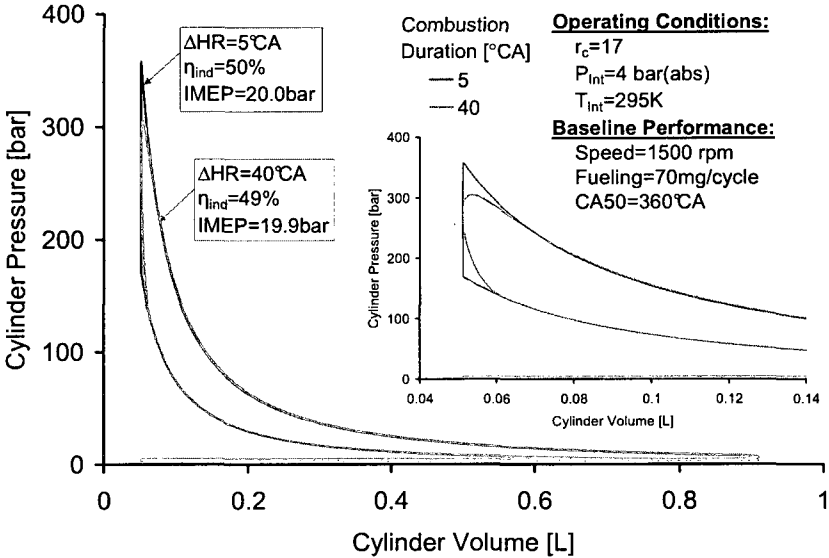


Figure 3-12: p-V diagram showing heat release duration effects

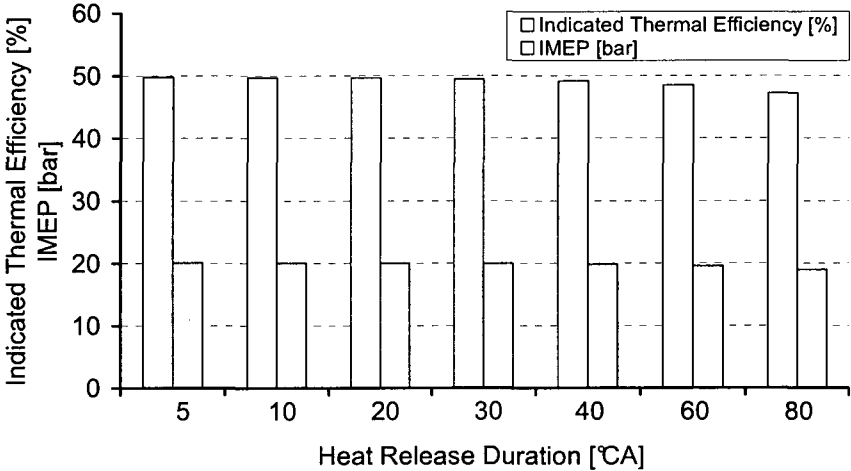


Figure 3-13: Heat release duration effects on engine performances

Finally, the combined effects of heat release phasing and duration on the indicated thermal efficiency is shown in Figure 3-14. The simulated heat release phasing is from 315 to 425°CA. The simulated heat release duration is from 5 to 80°CA. The optimum operating point with highest η_{ind} would be at the heat release position of 5°CA after TDC. It is the heat release phasing change that has a major influence on the η_{ind} . The η_{ind} for phasing change with different heat release durations follows the same trend over the range from 315 to 425°CA. Less than 3% decrease in η_{ind} has been observed when the heat release duration increases from 5 to 80°CA. Therefore, the heat release phasing has a stronger effect on the η_{ind} around TDC.

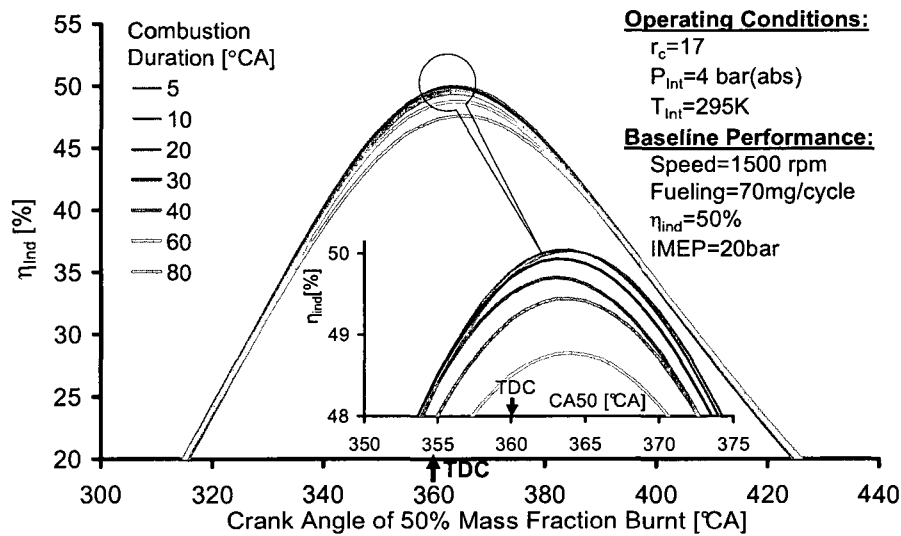


Figure 3-14: Effect of CA50 and heat release duration on η_{ind}

The effects of heat release phasing and duration on η_{ind} , maximum cylinder pressure (p_{max}) and maximum rate-of-pressure rise ($(dp/d\theta)_{max}$) is shown in Figure 3-15. The p_{max} increased as the CA50 advanced and the heat release duration shortened, while $(dp/d\theta)_{max}$ peaked at approximately 10°CA BTDC. In general, a short and advanced heat release rate may produce the combination of high p_{max} and $(dp/d\theta)_{max}$.

Excessively high p_{max} and $(dp/d\theta)_{max}$ may be beyond the design limit and cause the potential engine damage. The cylinder temperature also needs to be limited. The cylinder temperature must be high enough to complete the combustion, but not too high to avoid

increasing in NO_x emission. The reducing in both peak pressure and peak temperature results in the prolonging of the ignition delay. This is beneficial to HCCI engine operating due to the better mixing.

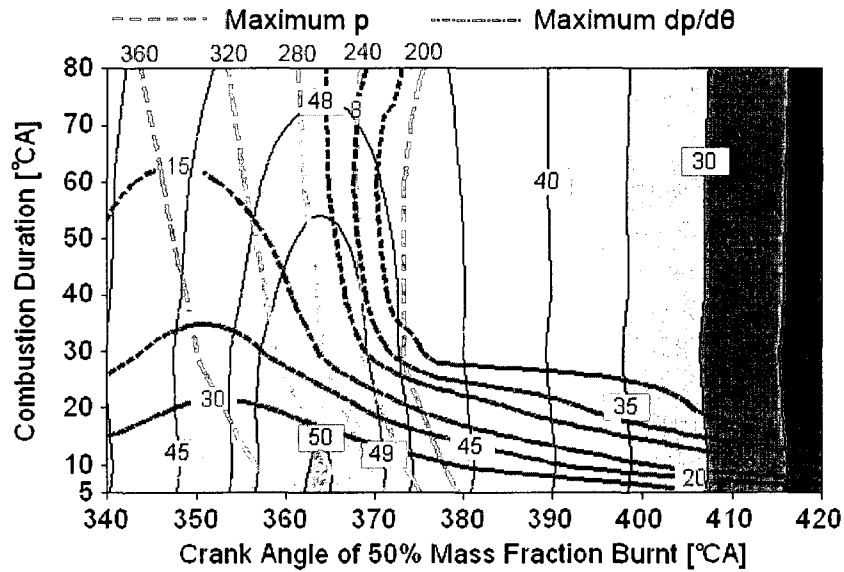


Figure 3-15: Effect of CA50 and heat release duration on η_{ind} , p_{max} and $(dp/d\theta)_{max}$

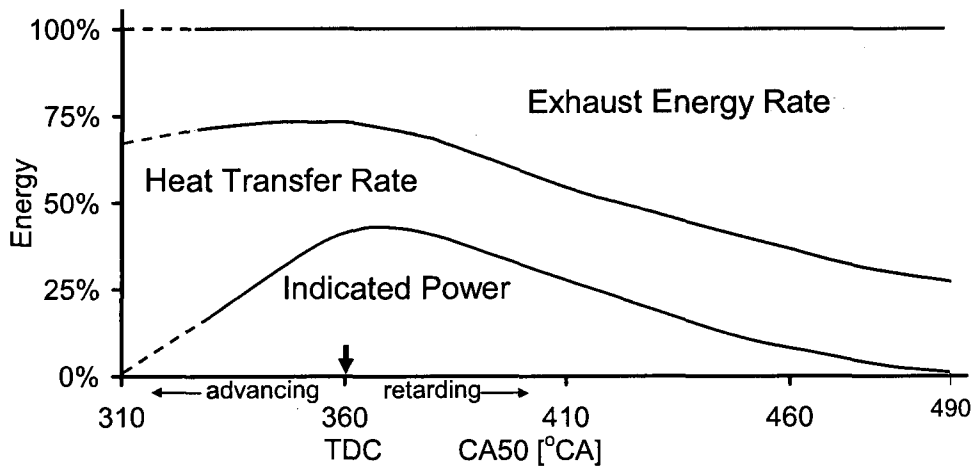


Figure 3-16: Effect of CA50 on indicated power, heat transfer and exhaust energy

As shown in Figure 3-16, under the above simulated conditions, the indicated power, or the indicated thermal efficiency, peaks at the CA50 position of approximately 5°CA ATDC. A large amount of fuel energy would be wasted when the combustion heat is

released too early, because an excess amount of heat would be lost to the engine coolant. When the combustion heat is released too late, an excess amount of heat energy goes to the exhaust.

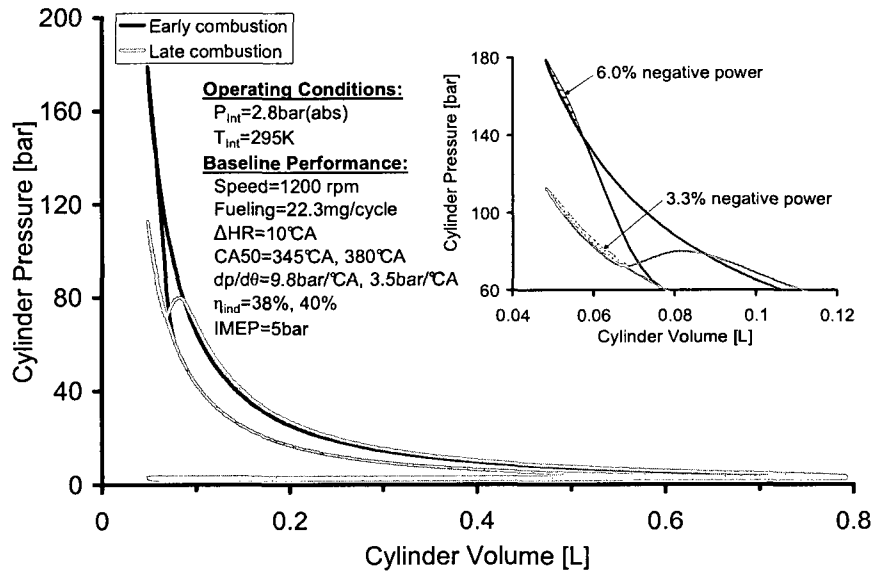


Figure 3-17: p-V diagram for early- and late-ignition combustion

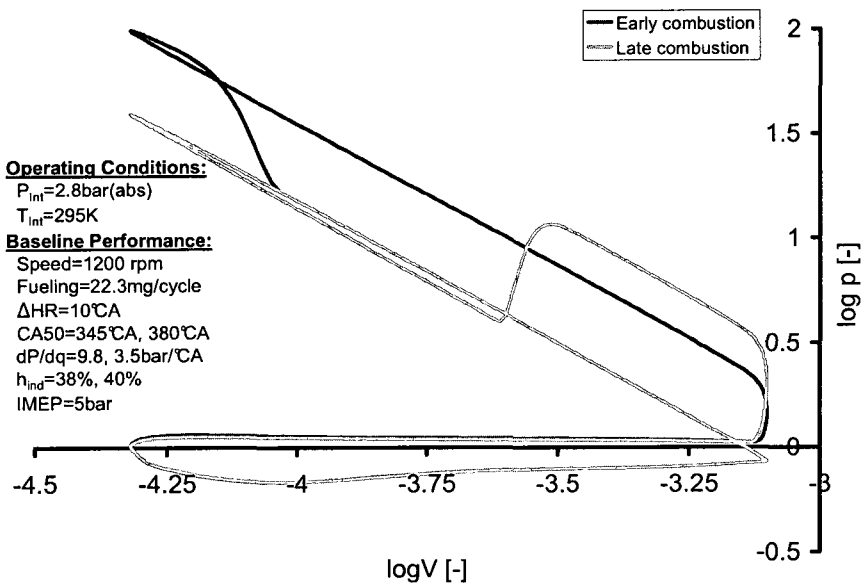


Figure 3-18: Logarithmic p-V for the early- and late-ignition combustion

The negative p-V work envelope incurred by the early or late heat release is considered insignificant as shown in Figure 3-17. When the CA50 is before 15°CA BTDC and 20°CA ATDC, the negative power is only a few percents of the total energy. The logarithmic p-V diagram is shown in Figure 3-18.

From control point of view, the heat release phasing, the CA50, is a practical feedback parameter to represent the combustion timing. To apply the feedback control with heat release phasing information, cylinder pressure sensors and the real-time computation are required.

3.2.2 Heat Release Shape Effects

Under the same operating conditions presented above, the heat release shape effects on the η_{ind} are analyzed for three representative heat release shapes provided in Figure 3-19. The black solid line (single hump shape) represents the heat release rate of LTC HCCI combustion case. The green dashed line (double hump shape) represents heat release rate of multiple injection case. And the red dotted line (long tail shape) represents the heat release rate of conventional diesel high temperature combustion case. For all the three cases, the heat release duration is at 30°CA and the CA50 is at 360°CA.

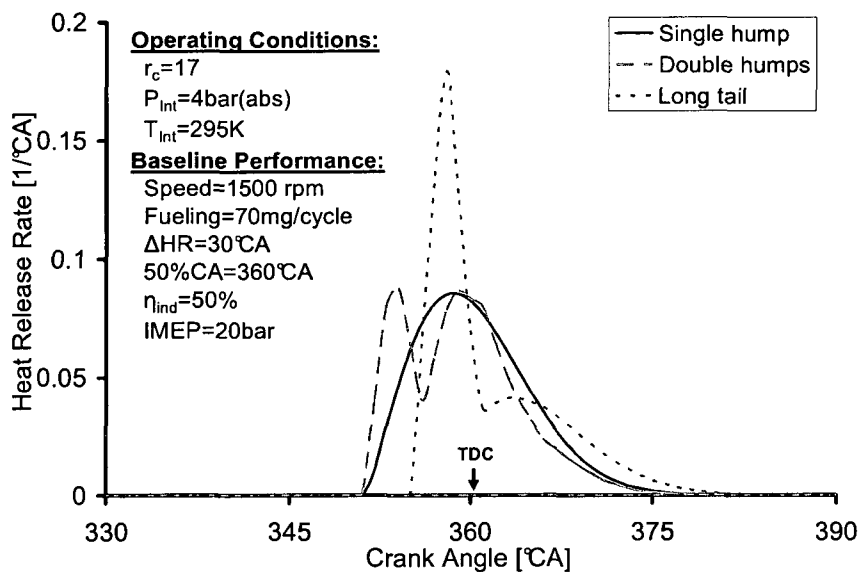


Figure 3-19: Specified input conditions with different heat release shapes

Furthermore, the simulated CA50 shifts from 340 to 420°CA while the heat release duration is kept at 30°CA. The simulation has been conducted for the three different heat release shapes respectively. The resultant η_{ind} is shown in Figure 3-20. It is noted that the η_{ind} is largely decided by the phasing effect and is insensitive to the heat release shape as the CA50 varies. It can be concluded that compared with the heat release phasing, the heat release shaping on the fuel efficiency may be insignificant.

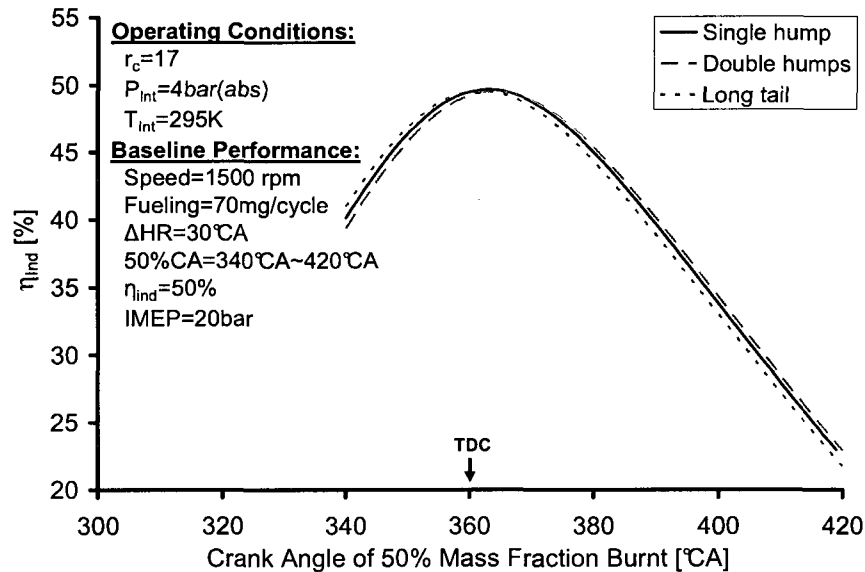


Figure 3-20: Effect of CA50 on η_{ind} for different heat release shapes with a fixed heat release duration

The above conclusion is valid for conditions with the fixed heat release duration of 30°CA. The effect of varying heat release duration also needs to be considered. Figure 3-21 shows the effect of CA50 and combustion duration on η_{ind} using the three different heat release shapes. The effect of the heat release shaping appears to gain significance when the heat release duration is greater than 40°CA. However, it is noted that the heat release duration of HCCI cycles is normally within 5~20°CA. Thus the conclusions drawn from the simulation results based on the Wiebe heat release rate shape are satisfying for the analyses [4,17].

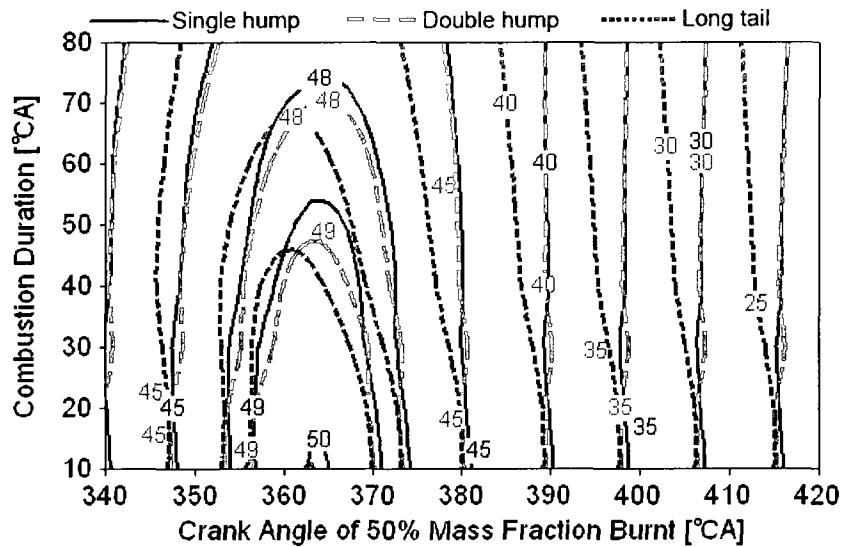


Figure 3-21: Map showing effect of CA50 and combustion duration on η_{ind} for different heat release shapes

3.2.3 Cylinder Pressure Characteristic Based Methods

Besides the heat release pattern, cylinder pressure characteristic is another indication of the engine performance. For applying the p_{max} -based or $(dp/d\theta)_{max}$ -based adaptive control, pressure sensor and real-time pressure data evaluation are required. The computational process is even simpler than the heat release calculation. The theoretical preparation for the control algorithm development is carried out by the simulation.

Figure 3-22 shows the simulation condition of a fixed heat release duration of 20°CA with heat release timing shifting from 340 to 420°CA progressively. The cylinder pressure traces emerge from a single peak to double peaks – the compression peak and the combustion peak. The timing of the peak pressure postpones progressively until the combustion peak falls below the compression peak [4].

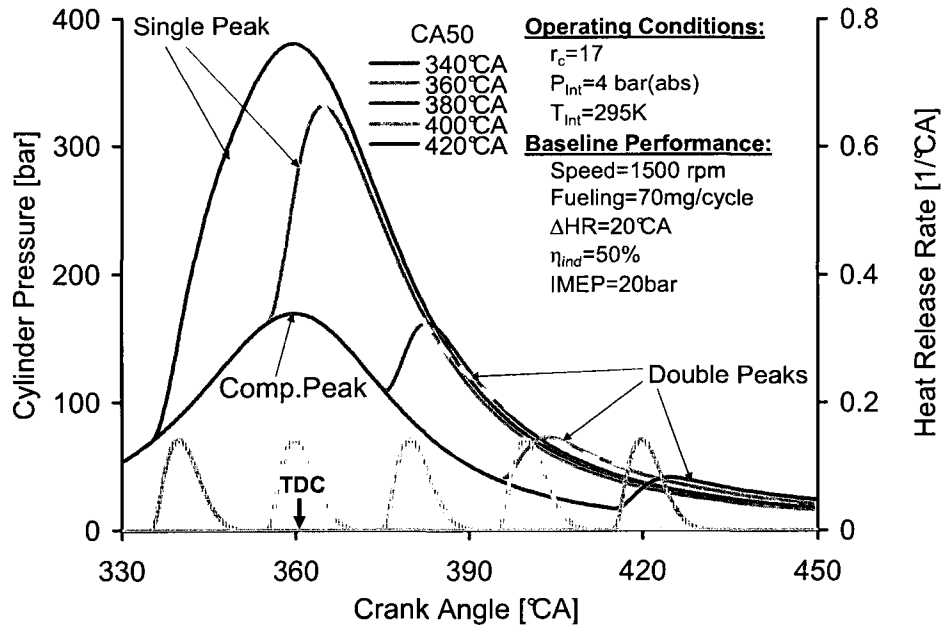


Figure 3-22: The cylinder pressure traces characteristics [4]

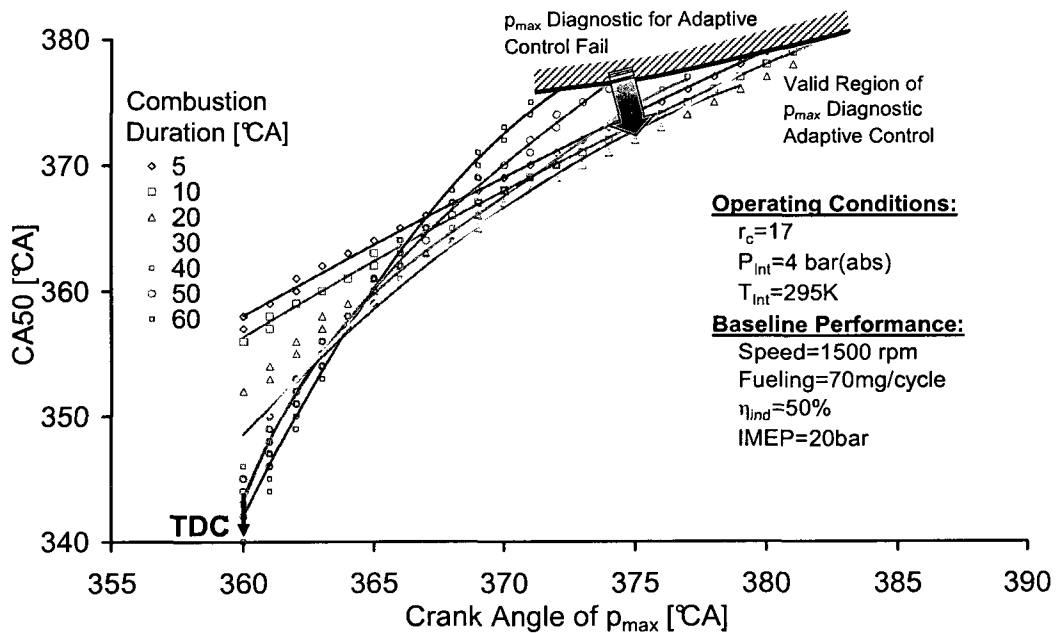


Figure 3-23: The correlation between CA50 and $\theta_{p_{max}}$ for different heat release durations [4]

The correlation between the crank angle of the maximum cylinder pressure ($\theta_{p_{max}}$) and the CA50 is shown in Figure 3-23, which is close to linear when the heat release duration

is relatively short. As the heat release widens, the valid range of the above correlation narrows. The correlation between the crank angle of the maximum rate-of-pressure rise ($\theta_{(dp/d\theta)_{max}}$) and the CA50 is even stronger, as shown in Figure 3-25. When the heat release duration is relatively short, the timing of the $(dp/d\theta)_{max}$ and the timing of CA50 almost occur concurrently. This correlation is valid until the rate of combustion pressure rise is lower than the rate of compression pressure rise, as shown in Figure 3-24. As the heat release widens, the valid range of the above correlation narrows [4].

Thus under the circumstances of shorter heat release duration, it is considered sufficient to approximate the heat release characteristics with the cylinder pressure characteristics. The simulation result further indicates that when the heat release is extremely late, which corresponding to an excessive postponing of the ignition time, the cylinder pressure trace could lose the identifiable features for the feedback control [4].

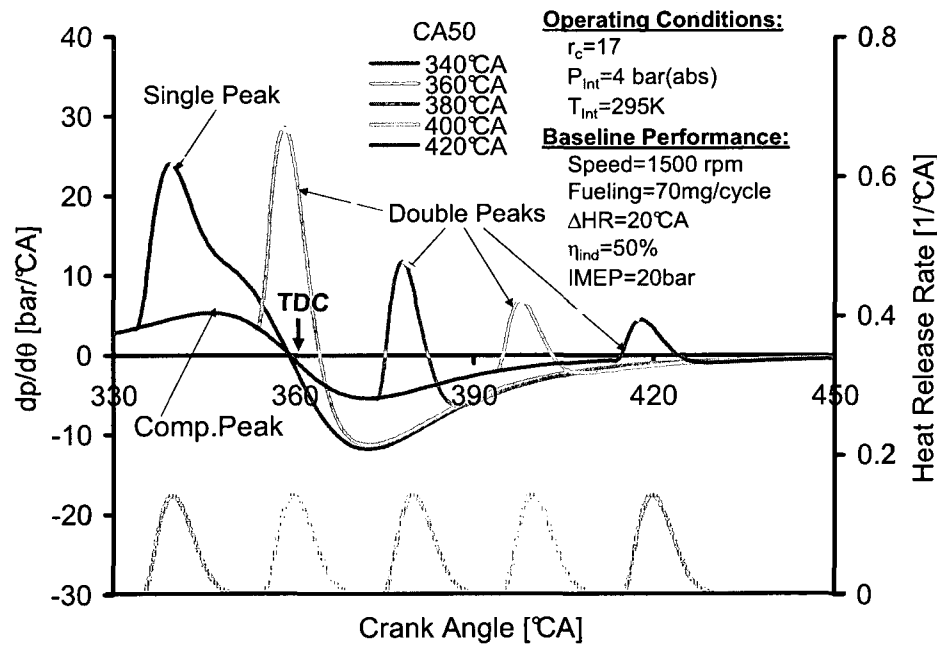


Figure 3-24: The rate-of-pressure-rise traces characteristics [4]

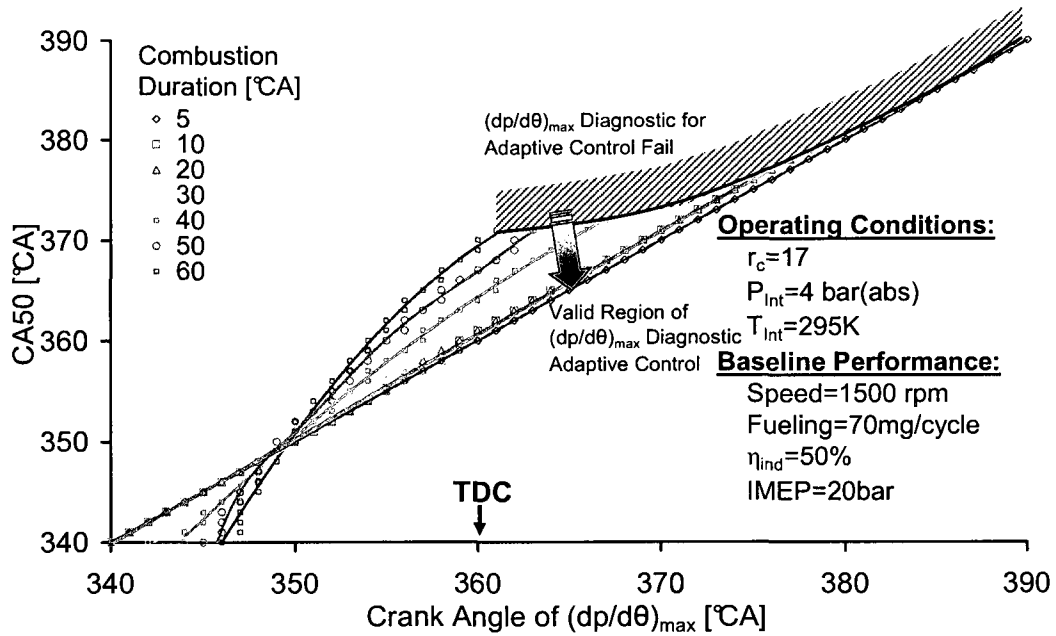


Figure 3-25: The correlation between CA50 and $\theta_{(dp/d\theta)_{max}}$ for different heat release durations [4]

The above conclusion is largely irrelevant to the heat release shape variations when the total duration of heat release is relatively short [4], for instance $\Delta HR \leq 20^\circ CA$. However, for wider or especially split heat release shapes, the timing correlation between the cylinder pressure characteristic and the CA50 shows noticeable difference as indicated in Figure 3-26 and Figure 3-27. The regions marked in blue and green represent the cases that the cylinder pressure characteristic loses identifiable features when the combustion is too early or too late respectively. By large the timing of the p_{max} and $(dp/d\theta)_{max}$ do not have a singular correlation with the timing of CA50, except within very narrow ranges as indicated in Figure 3-26 and Figure 3-27. In such cases, the substitution of the heat release analysis with the cylinder pressure characteristics become lesser confident and the heat release based adaptive control would be more suitable [4].

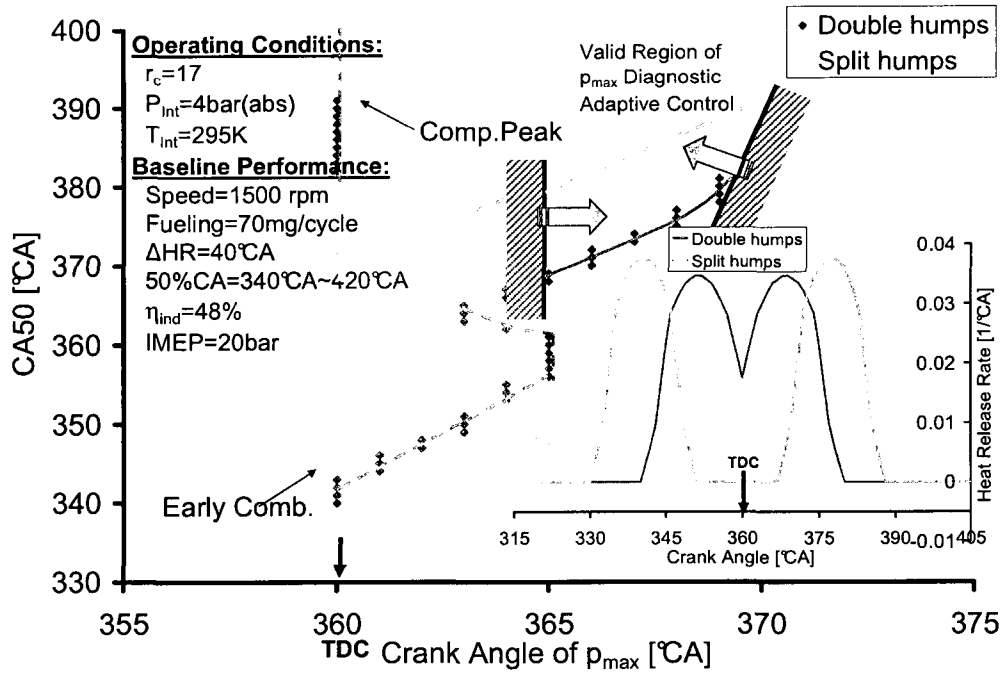


Figure 3-26: The correlation between CA50 and p_{max} for complex and split heat release rates [4]

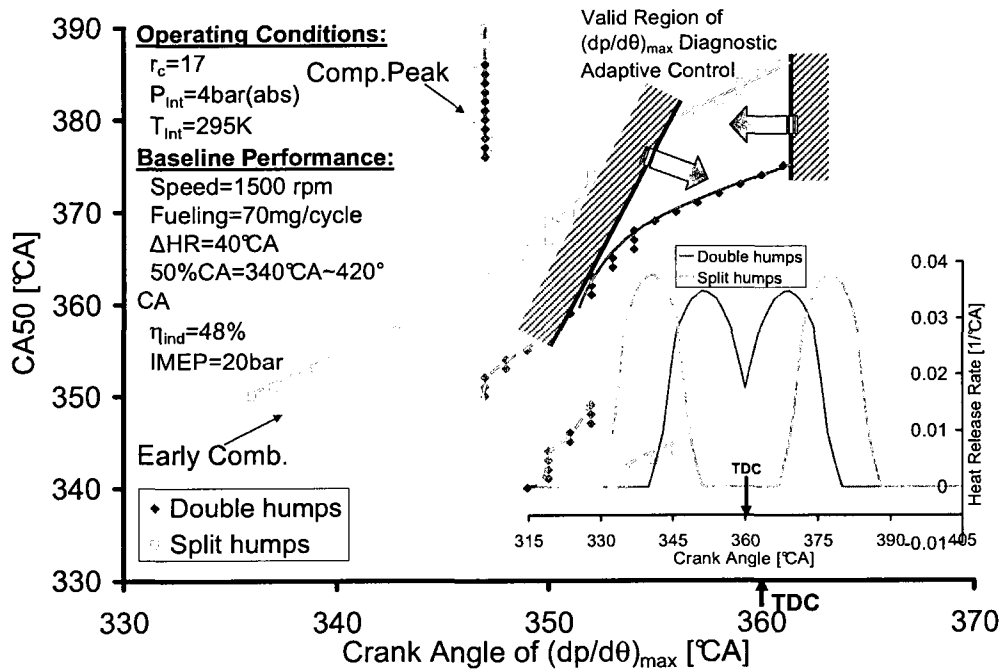


Figure 3-27: The correlation between CA50 and $\theta_{(dp/d\theta)_{max}}$ for complex and split heat release rates [4]

3.2.4 Compression Ratio Effects

The compression ratio effect is simulated by keeping the CA50 at 365°CA and the heat release duration at 30°CA. The engine speed is 1200rpm with intake pressure of 1bar(abs) and fueling rate of 22.3mg per cycle. Comparison is carried out by changing the compression ratio from 10:1 to 18:1. As shown in Figure 3-28, the cylinder pressure is strongly affected by the variations in compression ratio. As the compression ratio reduces from 18:1 to 10:1, the maximum cylinder pressure reduces by approximately 33bar (45%).

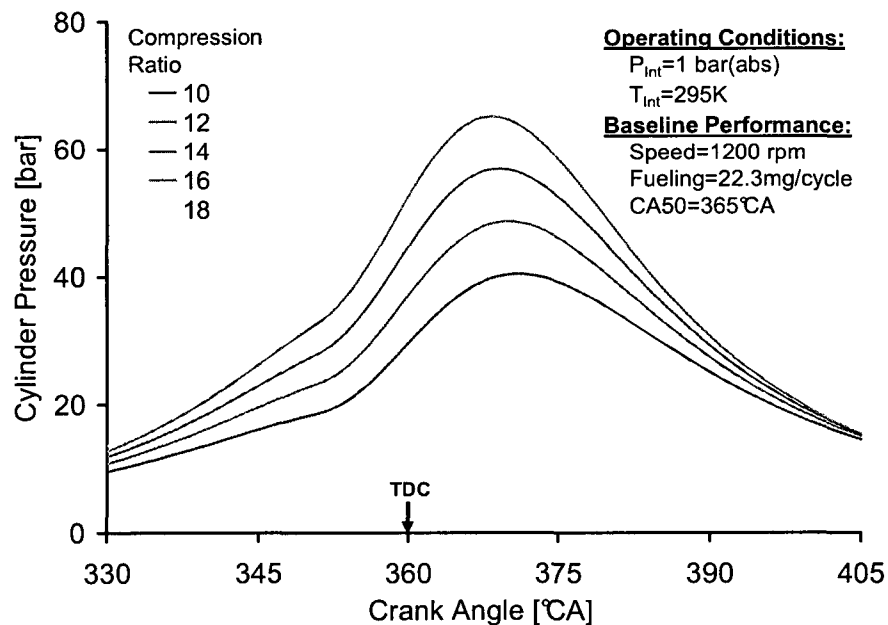


Figure 3-28: Cylinder pressure traces for different compression ratio

Figure 3-29 shows the effects of compression ratio on η_{ind} for different heat release phasing and duration. The heat release phasing shifts from 344 to 380°CA and the heat release duration varies from 10 to 40°CA. As demonstrated in the figure, the η_{ind} for different heat release phasing and duration follows the same trend as shown in previous section. The increasing in the compression ratio increases the indicated thermal efficiency for fixed heat release phasing and duration.

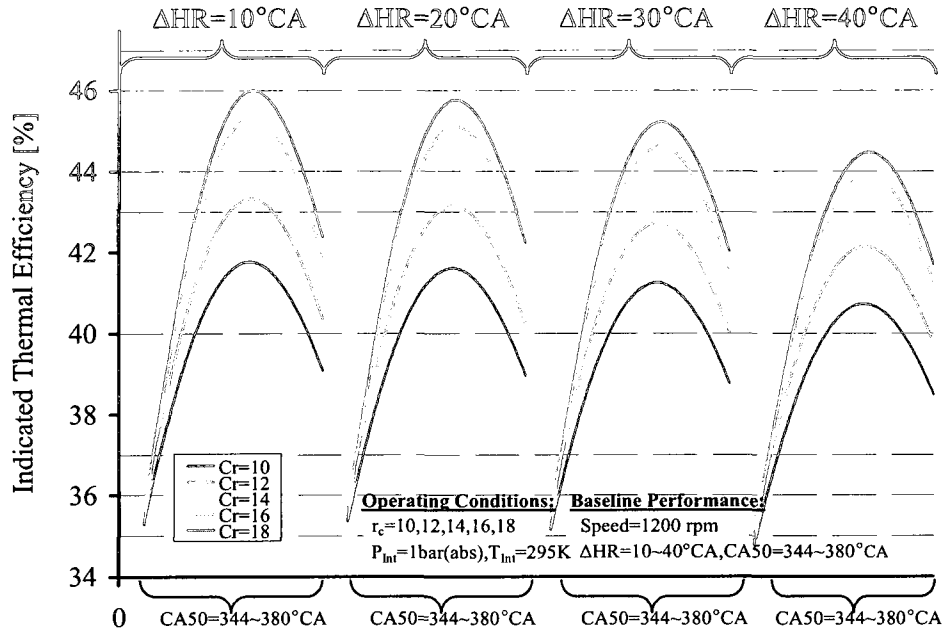


Figure 3-29: η_{ind} for different r_c and HR phasing and duration

Figure 3-30 shows the effect of CA_{50} and compression ratio on η_{ind} for a fixed heat release duration of $10^\circ CA$ (a detailed case from Figure 3-29). The highest η_{ind} occurs when the compression ratio increases to 18:1 and the CA_{50} is at a position of approximately $5^\circ CA$ ATDC.

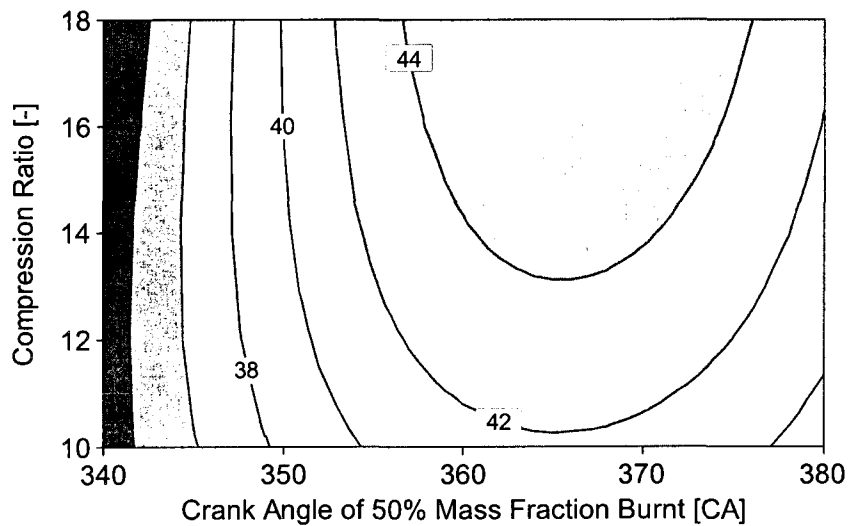


Figure 3-30: Map showing effect of CA_{50} and compression ratio on η_{ind}

Figure 3-31 shows the effect of CA50 and combustion duration on η_{ind} for compression ratios (r_c) 15:1 and 17.8:1. The higher compression ratio improves the efficiency significantly when the optimum heat release pattern is obtained. The optimum heat release pattern with the best efficiency is a combination of CA50 approaching approximately 5°CA ATDC and the duration is short (<30°CA). For longer durations or when the CA50 is far off from the combustion timing for the best efficiency, insignificant effects prevail with compression ratio variation.

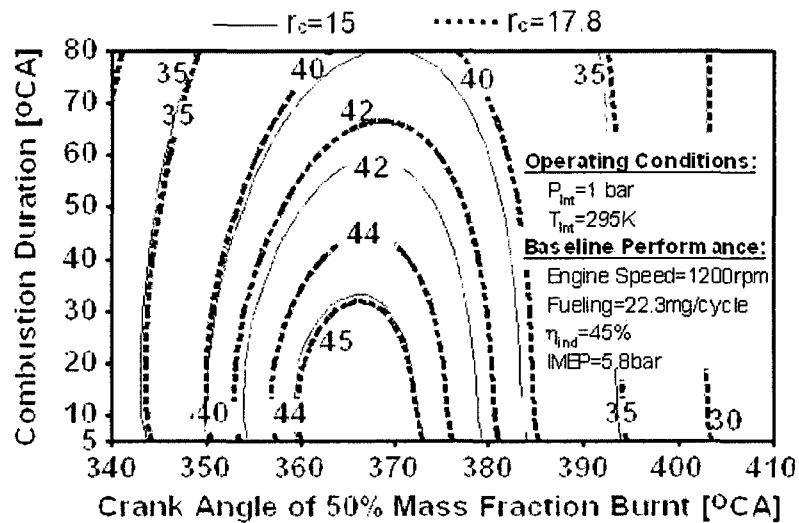


Figure 3-31: Map showing effect of CA50 and combustion duration on η_{ind} for compression ratios 15 and 17.8

CHAPTER IV

4 INDEPENDENT CONTROL OF EGR VALVE AND VCV, PCV

The independent control strategies of the EGR valve and rail pressure with substituting the original ECU control are discussed in this chapter. The independent control system is illustrated in Figure 4-1.

A Delphi® electronically actuated single-poppet rotary EGR valve is involved in the EGR flow control. The torque output of the valve is proportional to the current input. The EGR valve installation has been performed by fellow researcher Xiaoye Han. The EGR valve is controlled individually by different control strategies implemented in LabVIEW7.1. The rail pressure was originally controlled by the ECU through the volume-control valve (VCV) and the pressure-control valve (PCV). To perform independent control, the original control signal from the ECU is substituted by the signal generated from independent control programs. Dummy injectors have to be connected since the ECU checks the solenoid devices before allowing a normal engine operation.

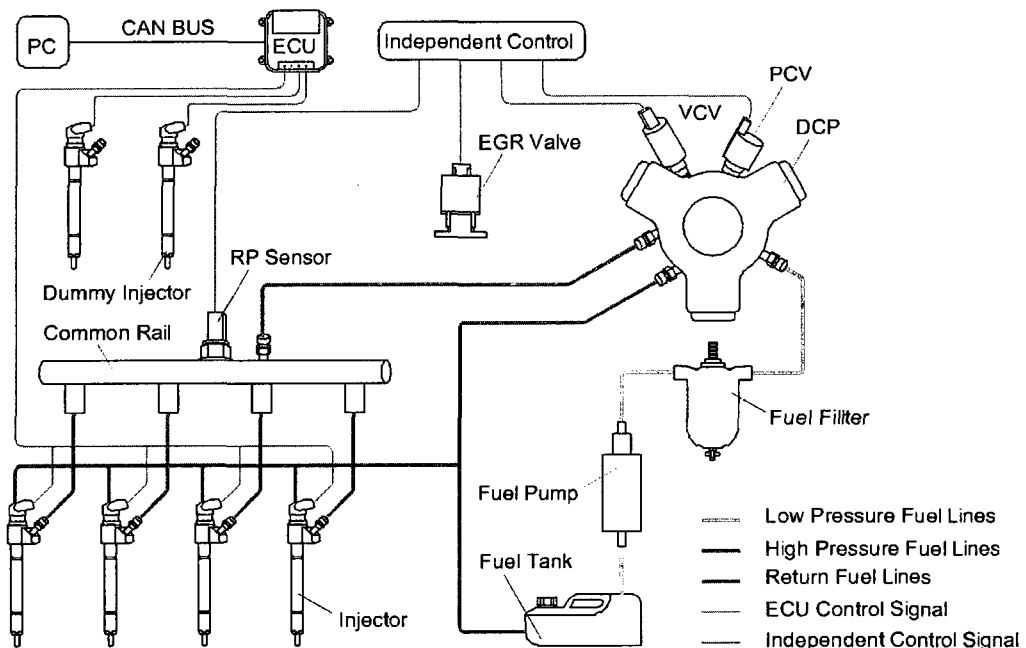


Figure 4-1: Independent control of EGR valve and common-rail pressure

4.1 Design and Methodology

As mentioned in Chapter Two, two fuel metering approaches of the rail-pressure control are listed in Table 4-1.

Table 4-1: Two fuel metering approaches

Fuel Metering Approaches	Volumetric Flow Approach	High Pressure Blow-off
Devices	VCV	PCV
Descriptions	Supplying Fuel Amount	Limiting Fuel Pressure

The EGR valve, the VCV and the PCV are electric solenoid actuated valves that are controlled by the valve electrical driver. Figure 4-2 shows the high-current motor driver circuit set-up in this research. The main part of this circuit is an H-bridge from POLOLU Corporation. The electrical driver controls the solenoid coil current with the PWM drive signal. The coil current can be controlled by adjusting the on-time or the duty cycle (D) of PWM drive signal through TTL signal generated from the programs.

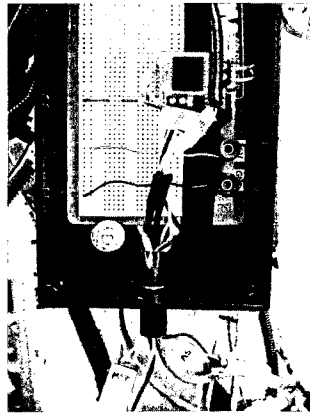


Figure 4-2: H-bridge circuit set-up in Clean Diesel Engine Laboratory

The EGR valve opening and rail pressure are determined by the position of the EGR valve body and VCV/PCV. To maintain the desired position of the valves, the feedback control loop monitors the actual valve position signal and updates the coils current correspondingly. The feasible feedback signals are exhaust valve position (EVP) sensor signal for the EGR valve control and rail-pressure signal for the VCV/PCV control.

The Delphi EGR valve comprises a contact-less EVP sensor shown in Figure 4-3. The position sensor is basically a potential meter that produces the feedback signal of the actual position of the valve body. As shown in Figure 4-4, EVP signal increases or decreases as a result of the EGR valve opening extent controlled by the duty cycle of the control current. Five terminals being used on the EGR valve are the motor positive and negative terminals, the position sensor signal terminal, the power supply terminal for the position sensor and the ground (GND) terminal [28].

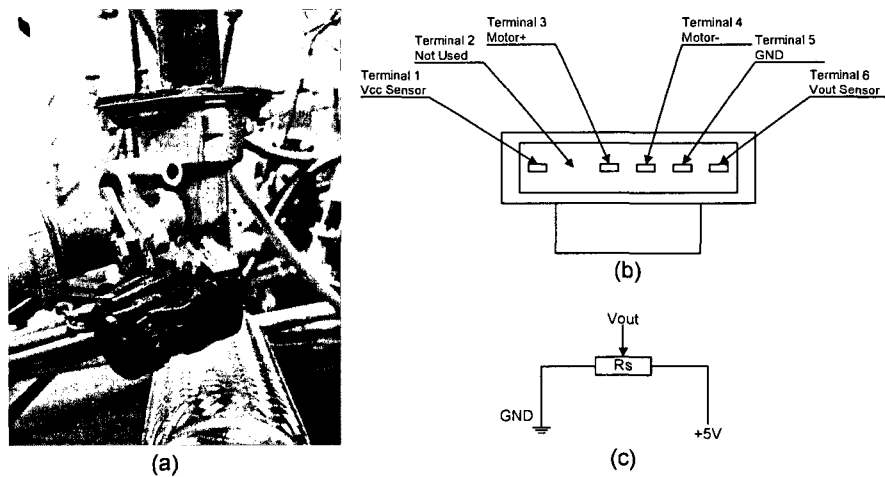


Figure 4-3: Empirical set-up of Delphi EGR valve in Clean Diesel Engine Laboratory (a), EGR valve terminals (b) and EVP scheme (c)

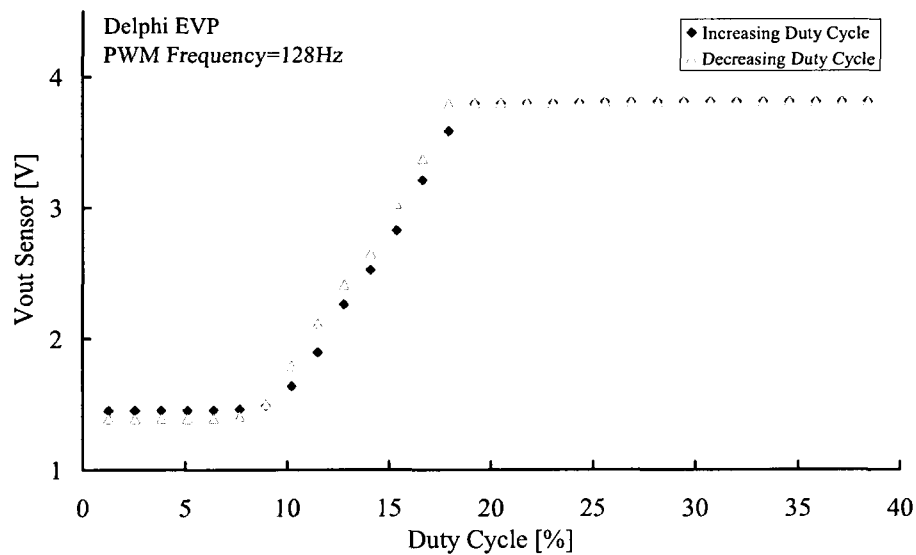


Figure 4-4: EGR valve position sensor response

As mentioned above, the control signal is in the form of PWM signal, while the set-point and feedback signal are voltage signals. Therefore, a computation process is necessary to control the duty cycle of the PWM signal according to the difference between the SP and the PV. A PID control algorithm is programmed in LabVIEW to realize the control functions shown in Figure 4-5 according to the PID control principles described in Chapter Two.

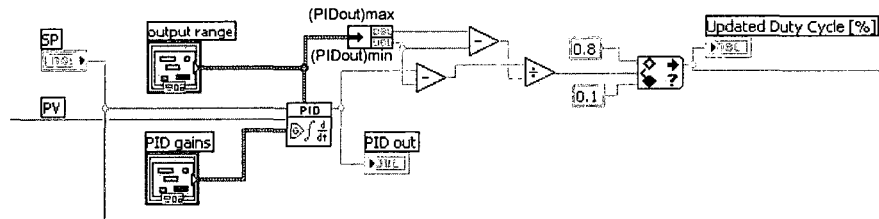


Figure 4-5: PID control block diagram in LabVIEW

The updated duty cycle of the PWM signal is determined by:

$$D[\%] = \frac{PIDout - PIDout_{min}}{PIDout_{max} - PIDout_{min}} \cdot 100\% \quad (4.1)$$

where, D is the duty cycle of the PWM control signal, $PIDout$ is the output of the PID algorithm and the $PIDout_{max}$ and the $PIDout_{min}$ are the pre-set maximum and minimum value of the PID control output. The updated duty cycle is further limited within the range of 10% to 80% to prevent solenoid coil overheating. The PWM signal with updated duty cycle is sent to Terminal 3 and Terminal 4 in Figure 4-3 to control the valve position.

4.1.1 EGR Valve Control

The schematic hardware implementation of the EGR valve control is shown in Figure 4-6 and the wiring connection is laid out in Figure 4-7. National Instrument (NI) PCI-6070E multifunction data acquisition card is implemented in the EGR valve control loop. The TTL signal generated from a counter card turns the H-bridge circuit ON and OFF to control the duty cycle of the PWM signal. The PWM control signal from the Out A and Out B Terminals of the H-bridge is sent to Terminal 3 and 4 of the EGR valve

respectively. The analog input channel of the data acquisition card acquires the feedback valve body position signal V_{out} from Terminal 6 of the EGR valve. The control computation to adjust the control signal according to the actual feedback condition is performed via the virtual instrument (VI) in LabVIEW that interacts with the data acquisition hardware.

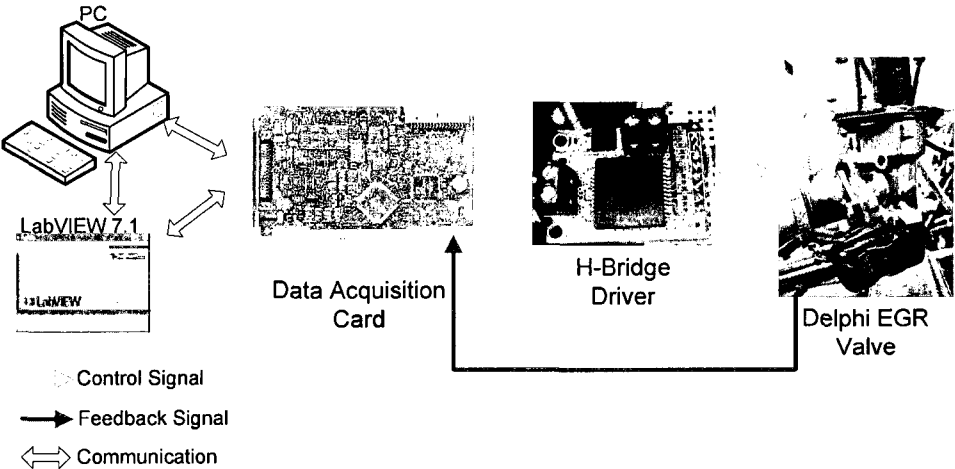


Figure 4-6: Empirical set-up of the Delphi EGR valve control

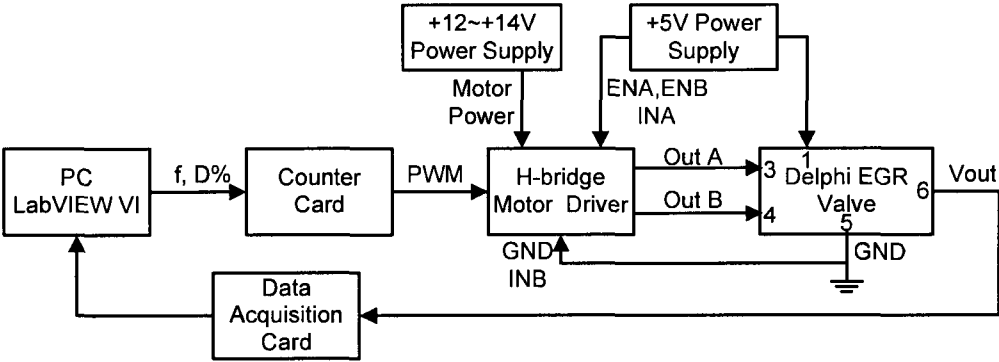


Figure 4-7: Detailed wire connection for Delphi EGR valve control

The deterministic control flowchart and the windows-style control program interface in LabVIEW7.1 are depicted in Figure 4-8 and Figure 4-9. The acquired actual valve position data is compared with the set-point and a compensating algorithm is applied to eliminate the disturbance and noises in order to maintain the targeted valve opening

position in real time. The data are also monitored graphically and recorded onto the hard drive in the background simultaneously.

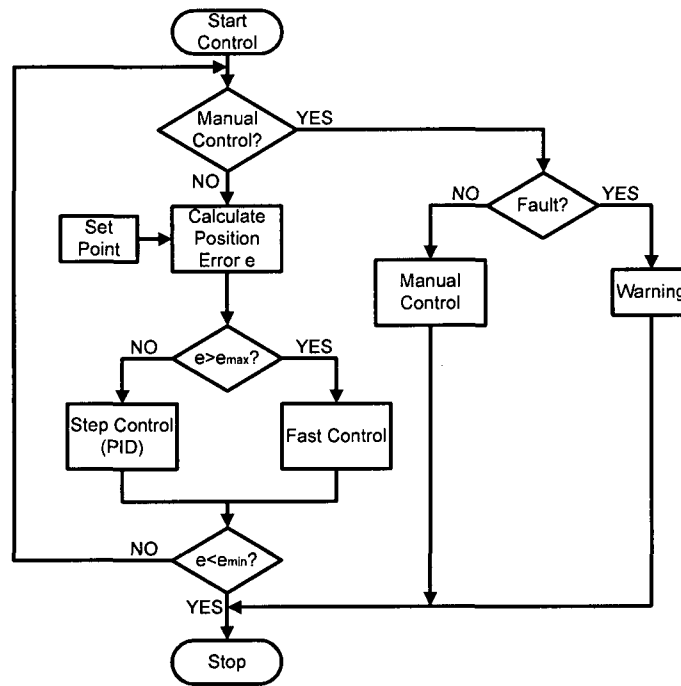


Figure 4-8: Algorithm flow chart of the Delphi EGR valve control program

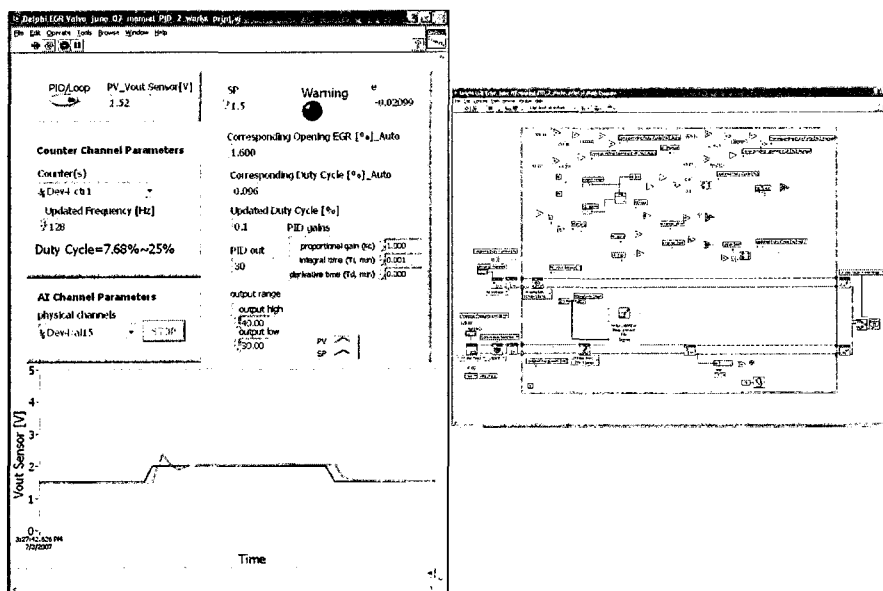


Figure 4-9: Front panel and block diagram for Delphi EGR valve control program

Besides the PID control algorithm, a fast compensation control is also implemented and tested, shown in Figure 4-10. Two operating limits can be set by the user to define the correcting speed. If the offset between the set-point and process variable is greater than upper limit, faster compensation is applied to correct the differences rapidly. Over-shooting occurs during the faster compensation. If the difference falls between the upper and the lower limit, a slower compensation is sufficient and precise for controlling the valve. If the difference is less than the lower limit, no compensation needs to be applied and the control outcome is satisfying.

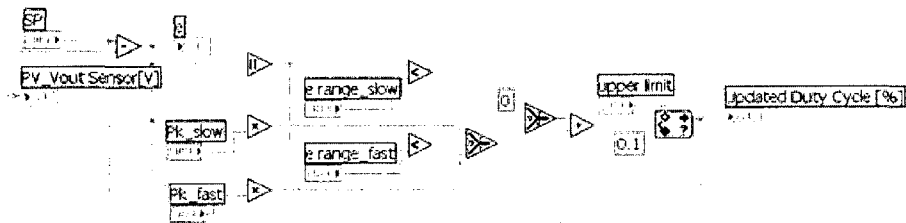


Figure 4-10: Fast compensation control algorithm block diagram in LabVIEW

4.1.2 VCV and PCV Control

Based on the operating principle, the common-rail pressure can be managed by VCV and PCV. For the fast and precise control, a real-time (RT) controller and high speed data acquisition cards are necessary. A schematic control diagram with NI cRIO-9002 RT module embedded with field programmable gate array (FPGA) for PCV control is shown in Figure 4-11. The cRIO RT module can be equipped with up to 8 individual hot-swap functional modules. The system set-up for current research is shown in Figure 4-11. The real-time controller NI cRIO-9002 has 8 slots with the NI cRIO-9401 and NI cRIO-9201 implemented in the first and seventh slot respectively. The ultra high-speed digital I/O module NI cRIO-9401 can generate TTL signals with various duty cycles as commanded to control the PWM signal output from the H-bridge circuit. The analog input module NI cRIO-9201 was used to receive the actual common-rail pressure signal which serves as a feedback signal. These control module set-ups were also used for many other on-going control activities in the Clean Diesel Engine Laboratory.

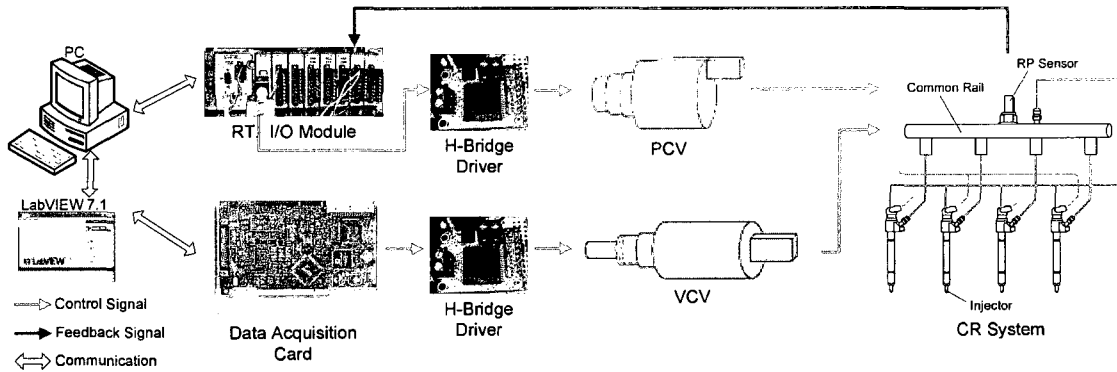


Figure 4-11: Schematic control set-up of the common-rail pressure control

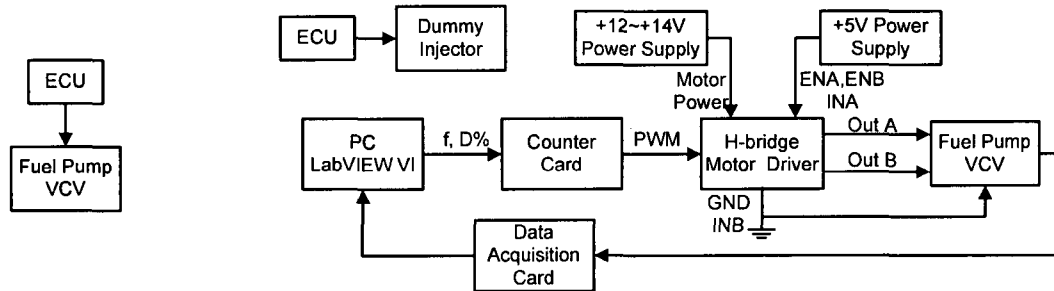


Figure 4-12: The original OEM set-up for VCV control (left) and the independent VCV control set-up (right)

The NI cRIO-9401 is a bidirectional digital module and the channels need to be configured as input or output channels respectively. The specifications of NI PCI-6070E, NI cRIO-9401 and NI cRIO-9201 cards are given in the APPENDIX A.

Similar to the EGR valve control, the TTL signal for VCV control is generated by a counter channel in NI PCI-6070E. The original VCV control and individually VCV control bypassing ECU are shown in Figure 4-12. The PWM signal generated from H-bridge, through Out A and Out B terminals, is sent to the Fuel pump VCV control terminals. The control program is shown in Figure 4-13. The counter channel generate TTL control signal with commanded duty cycle. The analog channel acquires actual fuel rail pressure.

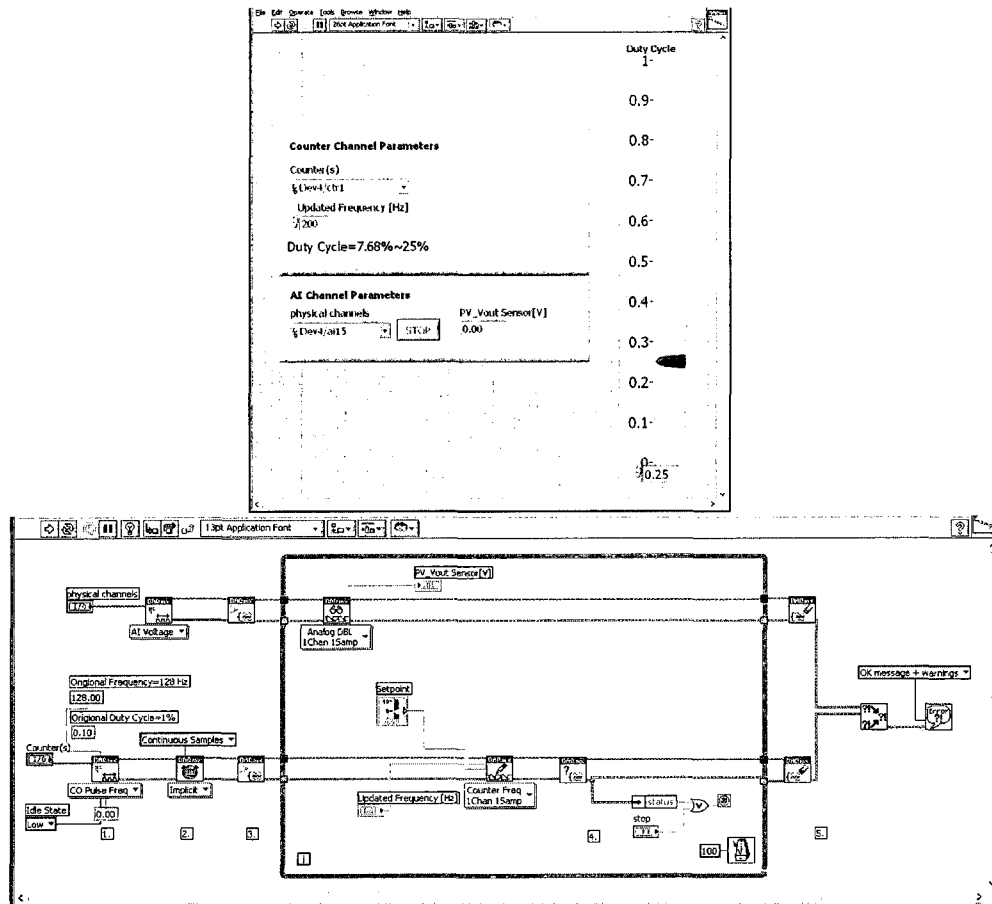


Figure 4-13: VCV control front panel (up) and block diagram (bottom)

The control program implemented in FPGA and empirical control set-up for PCV control are shown in Figure 4-14 to Figure 4-17. A PID control algorithm is applied to maintain the actual rail-pressure at the set-point. The control strategy is programmed on a real-time controller embedded with FPGA device by creating a control project consisted of a FPGA program and a real-time program. The LabVIEW can be configured to implement program in real-time controller or FPGA through target selection. The RT/FPGA targeting dialog and control project window are shown in Figure 4-15. The FPGA program generates TTL control signal and acquires actual fuel-rail pressure; the real-time controller performs the actual commanding control.

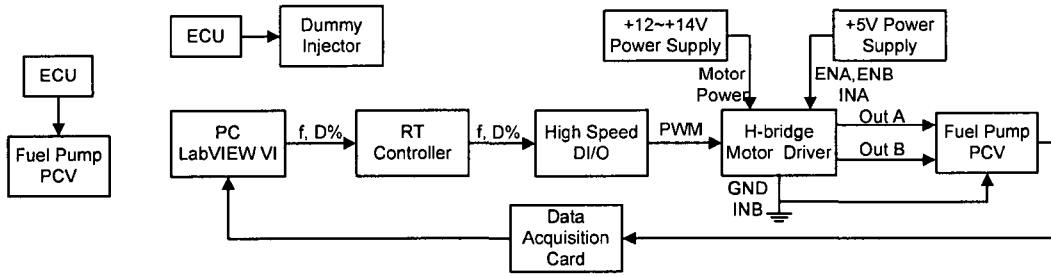


Figure 4-14: The original OEM set-up for PCV control (left) and the independent PCV control set-up (right)

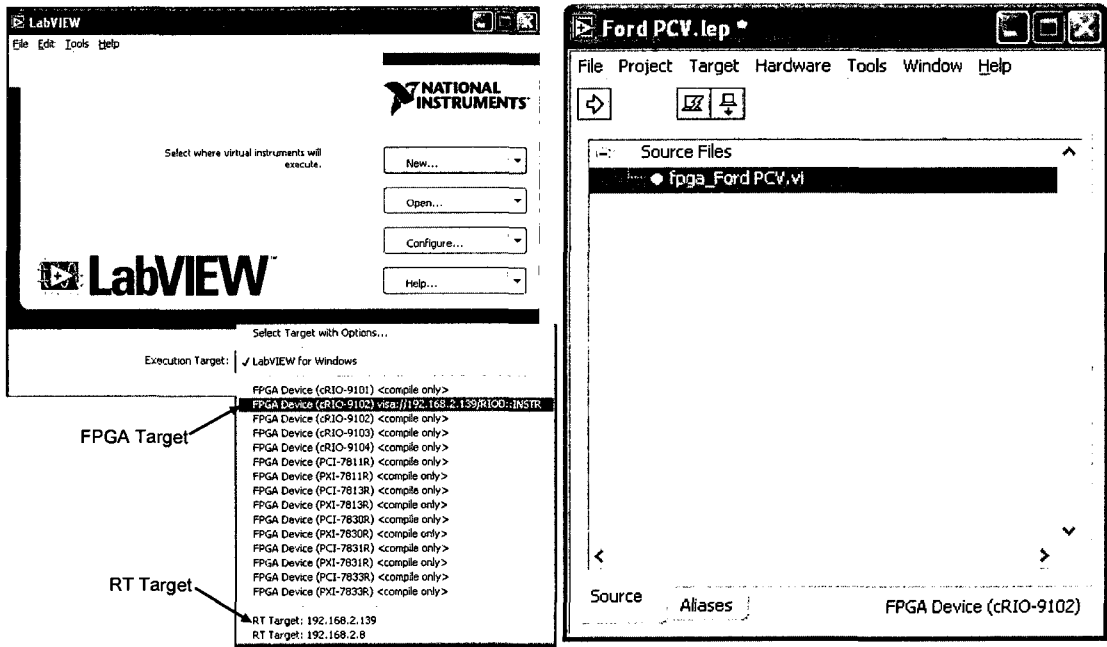


Figure 4-15: LabVIEW dialog window for selecting RT and FPGA target (left), project window (right)

The FPGA program shown in Figure 4-16 generates the TTL signal with commanded duty cycle and acquires actual rail-pressure signal from analog channel. For precise control, counter unit is set to a single clock cycle (ticks). The length of the clock cycle is determined by the clock rate for which the VI is compiled. For the compiling rate of 40MHz, the clock rate is $0.025 \mu s$. The counter units can be set to ticks and microseconds for FPGA Target and RT module. The real-time program in Figure 4-17 contains the computation algorithms. The actual rail-pressure signal is compared with the set-point.

The processed error signal adjusts the duty cycle of the PWM signal to eliminate the error and thus to achieve the commanded rail-pressure.

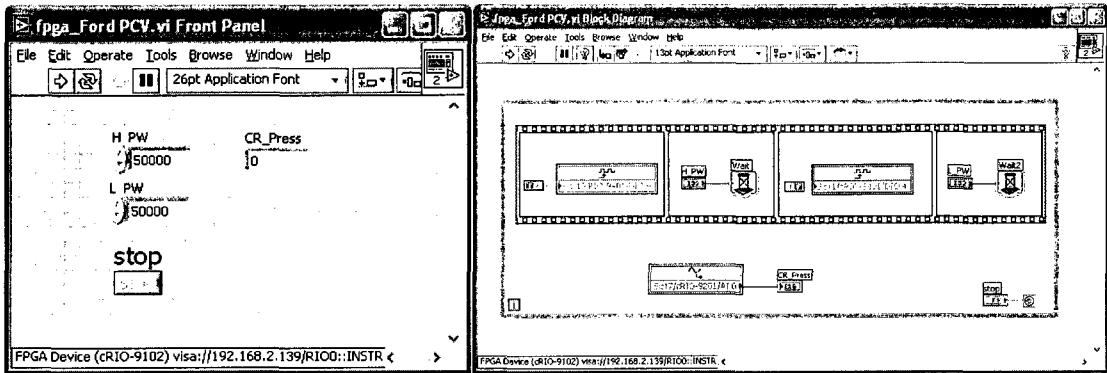


Figure 4-16: FPGA front panel (left) and block diagram (right) for PCV control

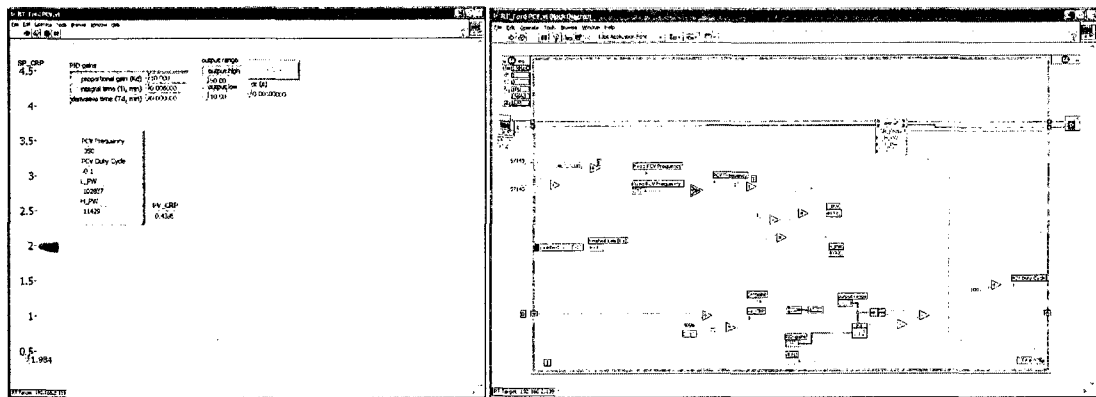


Figure 4-17: RT front panel (left) and block diagram (right) for PCV control

4.2 Empirical Results and Discussions

4.2.1 EGR Valve Control Empirical Results and Analysis

The comparison of the response to set-points between fast compensation control and PID control algorithms is shown in Figure 4-18. The test was conducted with the engine off so that there is no EGR gas flow disturbance. The EVP sensor output range is from +1.46V to +3.8V, representing valve fully closed and fully open correspondingly. The result from PID control has slightly slower response but less over-shooting compared to the fast compensation control.

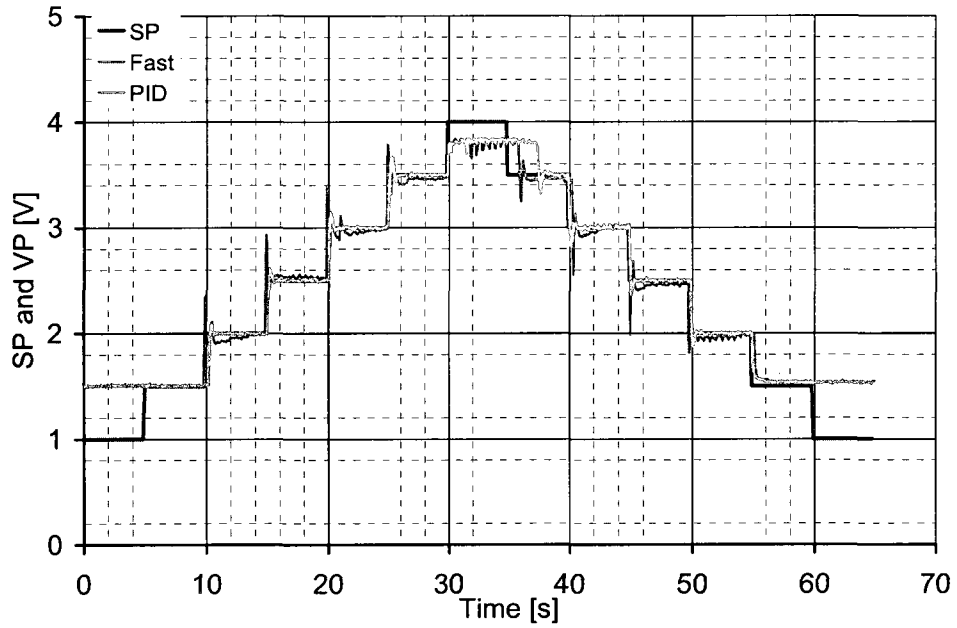


Figure 4-18: Comparison between different control algorithms

Figure 4-19 to Figure 4-21 show the empirical results of the EGR valve positions at commanded set-points during the engine test. Figure 4-19 indicates that the measured valve position follows the commanded set-point rapidly at the on-set of the control program. The minimum output value of EVP sensor is 1.46V when the EGR valve closes.

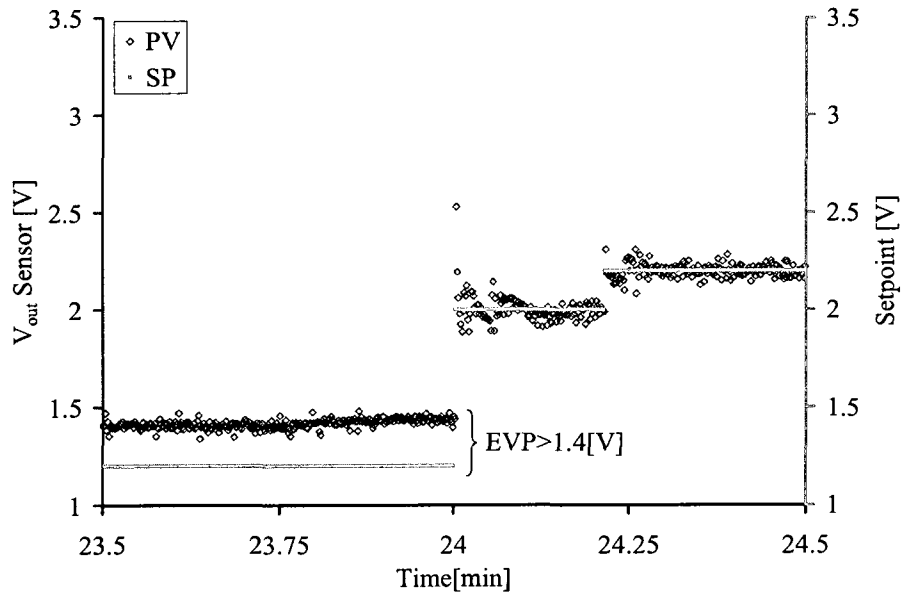


Figure 4-19: Empirical results of PID control with SP variations

Figure 4-20 shows that the set-point is closely maintained but with noticeable discrepancies during the tests. The discrepancy occurs because the spring force of the EGR valve is too weak to against the fluctuation of the flow pressures in the intake and exhaust manifolds.

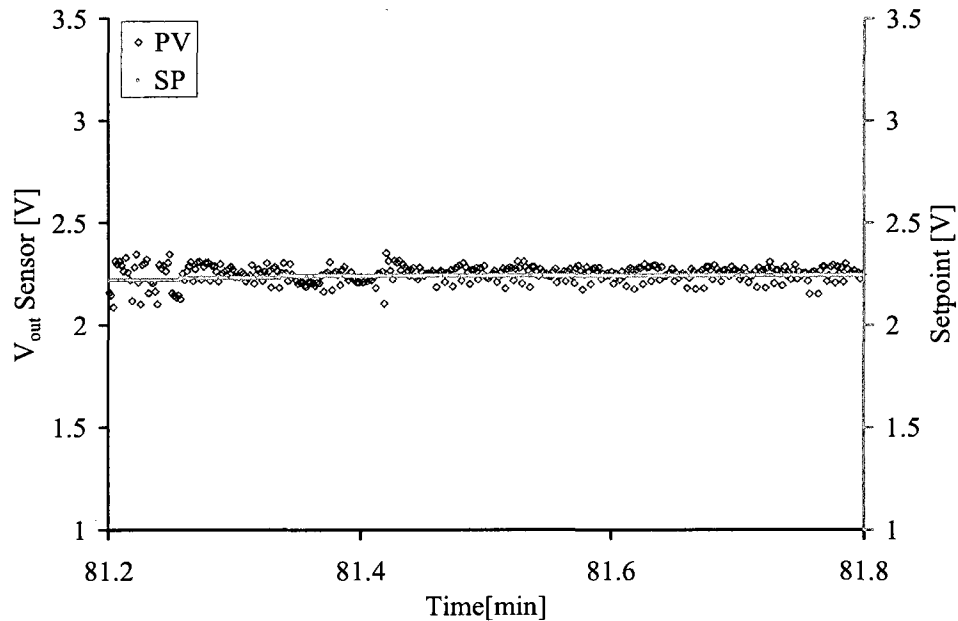


Figure 4-20: Empirical results of PID control under steady conditions

In cases, the discrepancy has been aggravated by the valve clogging and fouling under certain engine operating conditions such as low temperature combustion where the exhaust gas contain high amount of soot. The soot accumulated in the EGR valve causes EGR valve clogging and fouling thus delayed response and potentially valve malfunction as shown in Figure 4-21. However, the higher duty cycle of the control signal automatically produced by the control program has counteracted the valve sluggishness eventually. Figure 4-22 shows the EGR valve with soot accumulation and after cleaned with alcohol. The fouling problem may be improved by adding EGR oxidation catalyst (EOC) and/or implementing high force spring to ensure the accurate operating [26].

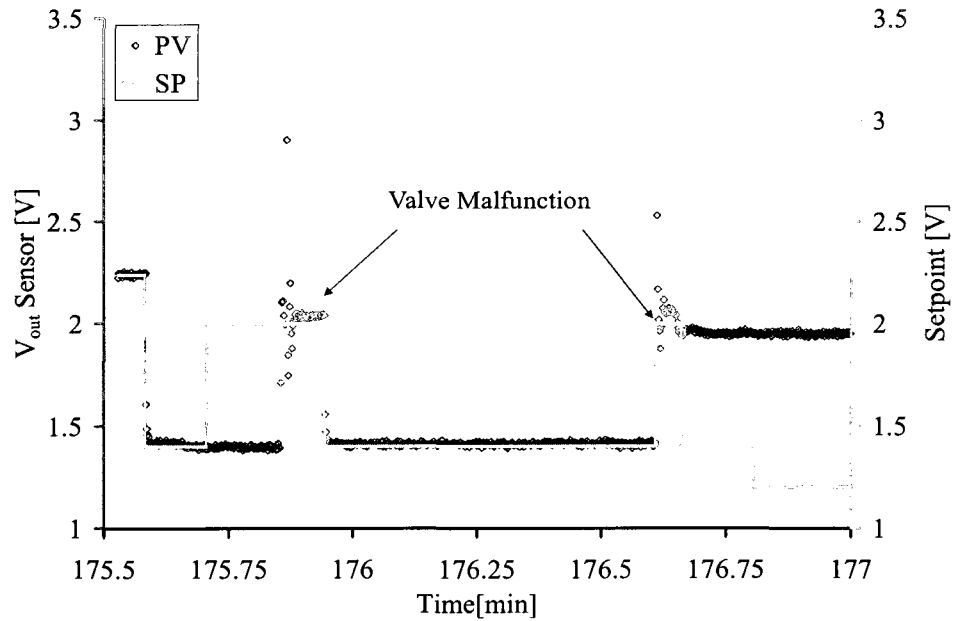


Figure 4-21: Empirical results of valve malfunction case

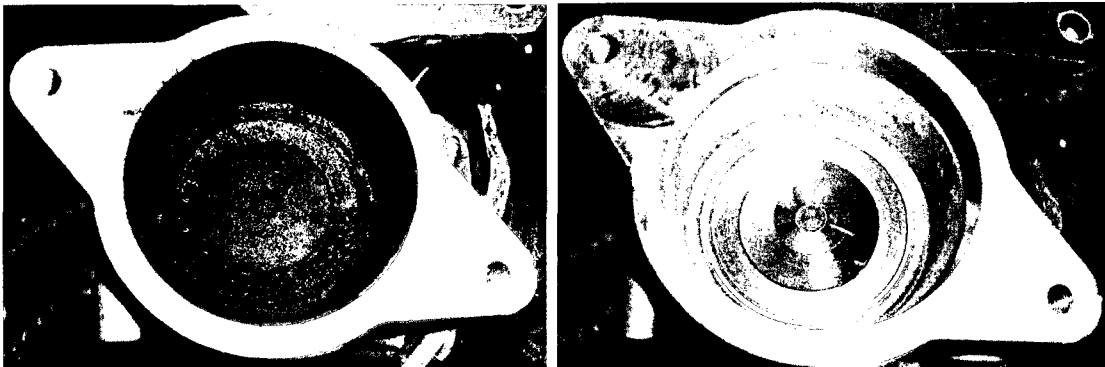


Figure 4-22: Soot accumulation on EGR valve (left), EGR valve after cleaning (right)

4.2.2 Rail Pressure Control Empirical Results and Analysis

By increasing the VCV and PCV control current, the common-rail pressure increases and thus the operating range of the injection pressure increases. As shown in Figure 4-23, to achieve the higher commanded common-rail pressure set-point, the duty cycle of the VCV PWM control signal should be increased to keep the VCV open for longer time and thus allow sufficient amount of fuel delivery. In addition, the duty cycle of the PCV

PWM control signal should be increased to keep the PCV closed for longer duration to build up high fuel rail pressure.

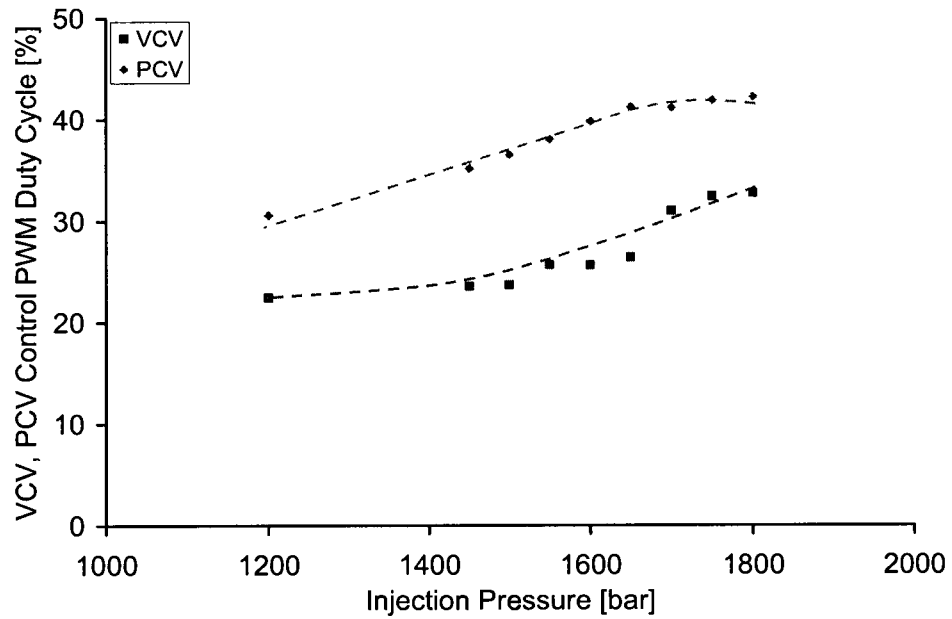


Figure 4-23: Duty cycle of PWM control current of VCV and PCV vs. injection pressure

CHAPTER V

5 CONCLUSIONS AND RECOMMENDATIONS

The objectives described in Chapter One have been achieved. Preliminary empirical and modeling analyses have been made to improve clean diesel combustion control. By performing zero-D engine cycle simulations, the impact of heat-release patterns on the fuel efficiency has been analyzed. Preliminary analyses have been made to correlate the maximum cylinder pressure and pressure rise with the combustion duration and phasing. Under the specified simulation conditions and assumptions, efforts are made to optimize the thermal efficiency of the engine. Overall, this thesis provides the modeling and empirical preparation that targets to improve diesel combustion control.

In the modeling work, the investigated parameters include the cylinder compression ratio and the phasing, duration, and shaping of heat release. Particularly, the strong impact of combustion phasing on fuel efficiency provides critical control boundary conditions for developing model-based engine control strategies. Additionally, the cylinder-pressure characteristic (p_{\max} and $(dp/d\theta)_{\max}$) analysis has been carried out for a simple and fast calculation [20]. The p_{\max} and $(dp/d\theta)_{\max}$ based control strategies have the potential to substitute HR-based control for certain operating conditions. In addition, the independent control of EGR valve, VCV and PCV has achieved satisfying outcomes.

In the empirical preparation part of this thesis, independent high-precision controls on the fuel pressure of the diesel common-rail system and the EGR valve opening have been accomplished by devising control algorithms that substitute the control from the ECU. A variety of control algorithms including manual feed-forward control, automatically fast feedback control and PID control have been implemented and tested to improve the response and precision of the EGR valve and the rail pressure control.

The following conclusions may be drawn from this research:

1. The simulated heat release patterns were demonstrated to be capable of describing the empirical heat release rate of diesel LTC cycles with sufficient conformity, in which the HCCI cycles tended to have early combustion.
2. The gain in energy utilization by the shortened apparent burning duration of diesel LTC operations in the investigated range is quantified as making insignificant improvement in the thermal efficiency from the modeling analysis.
3. The engine cycle simulation was considered helpful to identify the influencing parameters of diesel LTC efficiency. The simulation indicated that the phasing had the strongest, the duration the moderate and the shaping the weakest effects on thermal efficiency. In typical cases, when the CA50 was fixed at TDC, as the heat release duration increased from 5 to 40°CA the indicated thermal efficiency decreased from 49.5% to 47% only. In comparison, when the heat release duration was fixed at 5°CA, as the CA50 shifted from TDC to 10°CA BTDC the indicated thermal efficiency decreased from 50% to 45%.
4. The POLOLU high-power motor driver board incorporates most of the components of the typical application. The PWM control set-up is appropriate to control the solenoid devices such as EGR valve, VCV and PCV.
5. An independent rail-pressure control via VCV and PCV modulation was achieved by substituting the feedback and diagnostic signals of the existing ECU and by applying custom programs. Dummy injectors were utilized to bypass the original VCV and PCV control set-up.

The analytical work presented in this thesis has provided the preliminary preparation for an advanced model-based control work that the author is going to participate in. The next stage of this research will focus on the real-time adaptive control based on heat release pattern diagnostic and/or cylinder pressure characteristic recognition. The heat release pattern and cylinder pressure characteristic are used as the primary feedback control signals to adjust fuel injection scheduling. Based on the boundary operating conditions determined from the simulation analysis, the proper fuel injection control strategy will be

performed and then the heat release pattern will be reconstructed to progressively approach a set of desired heat release rate patterns to fulfill the emission, cylinder pressure, and combustion noise requirements.

Empirically, with the implementation of independent control of VCV and PCV, the common-rail pressure fluctuation because of the fuel injection events will be compensated to ensure the injection pressure so that the commanded fuel injection quantity is guaranteed. A variety of control algorithms and hardware integrations will be tested to contribute to the research theme of low temperature combustion with adaptive control of the Clean Diesel Engine Laboratory.

REFERENCES

1. Uwe Kiencke and Lars Nielsen, "Automotive Control Systems-For Engine, Driveline, and Vehicle", 2nd edition, Springer, 2005.
2. Rolf Isermann, Norbert Müller, "Design of Computer Controlled Combustion Engines", *Mechatronics* 13 (2003), pp.1067-1089.
3. Ming Zheng, Graham T. Reader and Hawley J.G., "Diesel Engine Exhaust Gas Recirculation-A Review on Advanced and Novel Concepts", *International Journal of Energy Conversion and Management*, Vol. 45, Issue 6, pp. 883-900, 2004.
4. Ming Zheng, Graham T Reader, **Yuyu Tan** and Meiping Wang, "Adaptive Combustion Control to Improve Diesel HCCI Cycle Fuel Efficiency", ASME paper No. ICEF2007-1630, p.8.
5. Seref Soylu, "Examination of Combustion Characteristics and Phasing Strategies of a Natural Gas HCCI Engine", *Energy Conversion and Management* 46 (2005), pp.101-119.
6. Hiroyuki Hiroyasu and Masataka Arai, "Structures of Fuel Sprays in Diesel Engines", SAE paper No. 900475, 1990, p.12.
7. Ming Zheng, "Thermodynamic Modelling and Experimental Investigation Experimental Investigation of a Synthetic Atmosphere Diesel Engine System", Ph.D. Thesis, University of Calgary, 1993.
8. Benson, Rowland Seider, "Internal Combustion Engines", 1st edition, Pergamon Press Inc. U.S.A., 1979.
9. J. Bengtsson, P. Strandh, R. Johansson, P. Tunestål and B. Johansson, "Closed-loop Combustion Control of Homogeneous Charge Compression Ignition (HCCI) Engine Dynamics", *International Journal of Adaptive Control and Signal Processing*, Int. J. Adapt. Control Signal Process. 2004; 18: pp.167-179 (DOI: 10.1002/acs.788).

10. Gregory J. Hampson, "Heat Release Design Method for HCCI in Diesel Engines", SAE paper No.: 2005-01-3728, p.9.
11. H. Husted, D. Kruger, G. Fattic, G. Ripley and E. Kelly, "Cylinder Pressure-Based Control of Pre-Mixed Diesel Combustion", SAE paper No. 2007-01-0773, p.6.
12. BOSCH, "Diesel-Engine Management", 3rd edition, SAE International, 2004.
13. Andrea Balluchi, Antonio Bicchi, Emanuele Mazzi, Alberto L. Sangiovanni Vincentelli and Gabriele Serra, "Hybrid Modelling and Control of the Common Rail Injection System", Springer-Verlag Berlin Heidelberg 2006.
14. Siemens VDO, "Piezo Common Rail Diesel System-Restricted Documentation", 2003.
15. National Instrument, "PID Control Toolkit User Manual", 2006.
16. ExperTune Inc., "What Is PID-Tutorial Overview", <http://www.expertune.com/tutor.html>, Accessed on July 11, 2007.
17. Ming Zheng, **Yuyu Tan**, Mwila Clarence Mulenga, and Meiping Wang, "Thermal Efficiency Analyses of Diesel Low Temperature Combustion Cycles", SAE paper No. 07FFL-10, p.9.
18. Heywood JB. Internal combustion engine fundamentals. McGraw-Hill Inc.; 1988.
19. Xiaoye Han, Usman Asad, Raj Kumar, Mwila Clarence Mulenga, Siddhartha Banerjee, Meiping Wang, Graham T. Reader, Ming Zheng, "Empirical Studies of Diesel Low Temperature Combustion on a Modern Diesel Engine", Combustion Institute/Canadian Section, Spring Technical Meeting, Session-H4, pp.1-7.
20. Raj Kumar, Ming Zheng, Usman Asad and Graham T. Reader, "Heat Release Based Adaptive Control to Improve Low Temperature Diesel Engine Combustion", SAE 2007 World Congress, paper 2007-01-0771, SP2087, pp.13-20.

21. Ming Zheng, Graham T. Reader, “Adaptive Control to Improve Low Temperature Diesel Engine Combustion”, 2006 Diesel Engine Emission Reduction Conference (DEER), Oral presentation, Detroit, MI, USA; August 20-24 2006, Available on Line at http://www1.eere.energy.gov/vehiclesandfuels/pdfs/deer_2006/session8/2006_deer_zheng.pdf.
22. **Yuyu Tan**, Mwila Clarence Mulenga, Usman Asad, Meiping Wang, Graham T. Reader and Ming Zheng, “Preliminary Analysis of Fuel Efficiency of Diesel HCCI Cycles”, Combustion Institute/Canadian Section, Spring Technical Meeting, 2007, Session D, p.8.
23. Hiroyasu H. and *et al.*, “Total In-cylinder Sampling Experiments on Emission Formation Process in a DI Diesel Engine”, SAE Paper No. 902062, 1990, p10.
24. Kevin P. Duffy, William L. Hardy and Michael P. Liechty, “Effects of Fuel Property Changes on Heavy-Duty HCCI Combustion”, SAES paper NO. 2007-01-0191, pp.143-155.
25. Yuuichi Kodama, Izumi Nishizawa, Takumi Sugihara and Norihiko Sato, “Full-Load HCCI Operation with Variable Valve Actuation System in a Heavy-Duty Diesel Engine”, SAE paper No. 2007-01-0215, pp.451-461.
26. Ford, “2008 6.4L Super Duty Overview”, <http://www.forddoctorsdts.com/bulletins/20086.4LOverviewLight.ppt#27>, Accessed on July 16, 2007.
27. National Instrument, “LabVIEW 8 FPGA module training materials”, 2007.
28. Delphi Corporation, “Diesel Single Poppet Rotary EGR Product Overview”, 2003.
29. Pololu Corporation, “Pololu High-Current Motor Driver Carrier”, <http://www.pololu.com/products/pololu/0705/>, Accessed on April 26, 2007.
30. MCE-5 Development, “Main VCR Technologies Principles, Advantages and drawbacks”,http://www.mce-5.com/vcr_strategy/vcr_engines_principles.htm, Accessed on July 11, 2007.

31. Miro International Pty Ltd., "Exploring Mazda's Intake Technology", 2004, http://www.mazda6tech.com/index.php?option=com_content&task=view&id=14&Itemid=1, Accessed on July 10, 2007.
32. "Engine, PowerTech Plus™ 9.0 L External, Efficiency, and Performance Features", 2006, http://salesmanual.deere.com/sales/salesmanual/en_NA/tractors/2006/feature/engine/8030/8030_9l_engine_external_efficiency.html, Accessed on July 10, 2007.

APPENDIX A. DEVICE CONFIGURATIONS AND SPECIFICATIONS

The relevant specifications of data acquisition devices from National Instrument are summarized and listed in this section. Important configuration and computation methods are also discussed.

Table A-1: Specifications of NI PCI-6070E

Analog Inputs	16-channel, 12-bit, 1.25MS/s
Input Range	$\pm 0.05 \sim \pm 10V$
Analog Outputs	2-channel, 12-bit, 1MS/s
Output Range	$\pm 10V$
Digital I/O	8-channel
Counters	2-channel, 24-bit

The NI 9401 is a bidirectional digital module and the channels need to be configured to be input or output respectively. The specifications of NI cRIO-9401 are shown in Table A-2 and the channel configuration window is illustrated in Figure A-1.

Table A-2: Specifications of NI cRIO-9401

Digital I/O	8-channel, 5V/TTL, bidirectional
Max Output Rate	100ns
Output Current per Channel (mA)	2
Connector Options	Industry-standard 25-pin D-Sub Connector

Table A-3: Specifications of NI cRIO-9201

Analog Inputs	8-channel, Single-ended
Input Range	$\pm 10V$
Aggregate Sampling Rate	500 kS/s
Resolution	12-bit
Connector Options	Screw Terminal or D-Sub Connectors

The labVIEW FPGA module utilizes integer for mathematical operations. That is, analog output operations with Compact RIO utilize the binary code representation of the desired output voltage. The conversion between the binary code and the desired output voltage follows equation (A.1):

$$\frac{\text{BinaryCode}}{2^{\text{Module Resolution [Bits]}}} = \frac{V_{\text{out}}}{\text{OutputRange}} \tag{A.1}$$

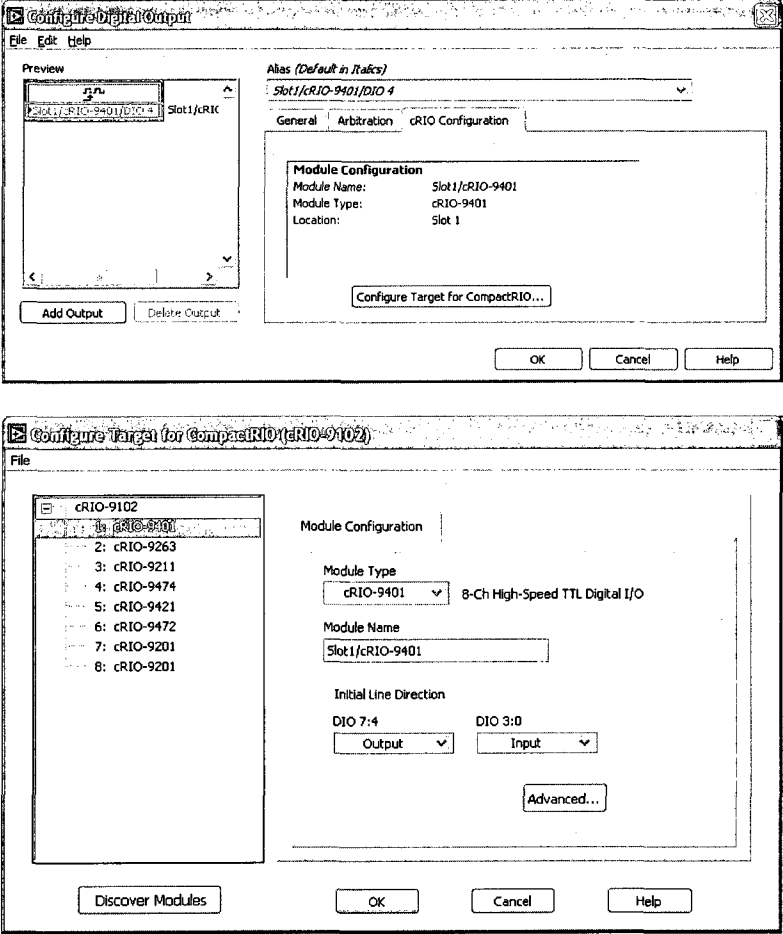


Figure A-1: Channel configuration of NI cRIO-9401

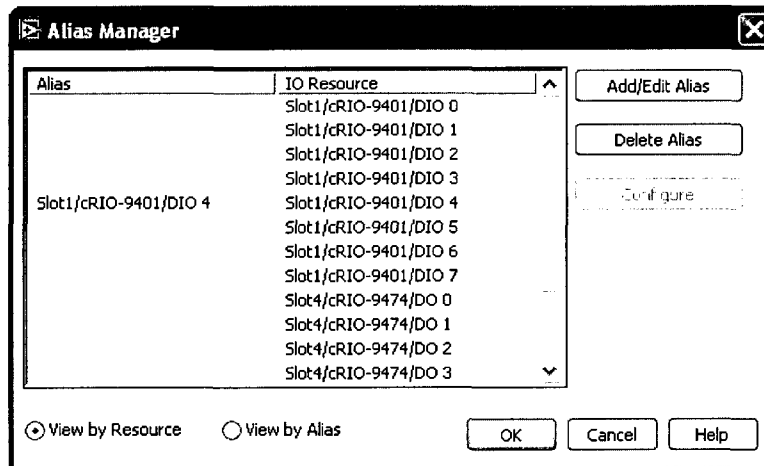


Figure A-2: FPGA channel selection

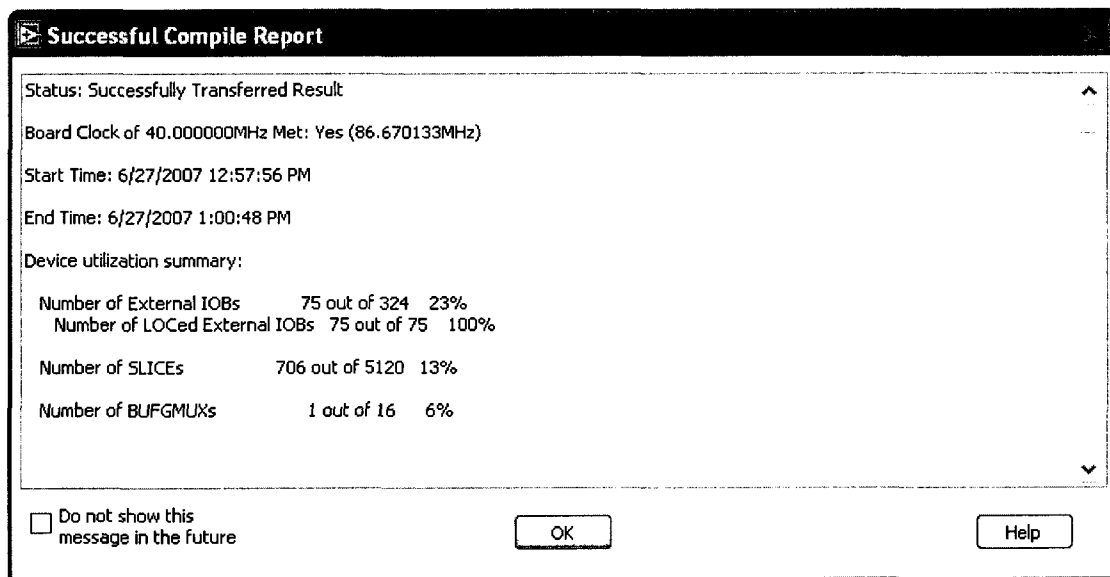


Figure A-3: FPGA successful compile report

IOBs: Input/Output Blocks

SLICES: Combination of look-up tables (LUTs) and flip flops (FFs)

BUFGMUXs: portal to the clock net, which is used to clock FFs [27]

APPENDIX B. DELPHI EGR VALVE SPECIFICATIONS

Table B-1: Specifications of Delphi EGR Valve [28]

Description	Electronically Actuated EGR Valve for Diesel and High Flow Gasoline Applications
Open Time / Close Time	<50ms / <50ms
Nominal Voltage	13.5VDC
Operating Voltage Range	0~16VDC
Operating Temperature	-30~135°C
Max Gas Temperature at Valve	400°C-60kg/h
Max Actuator Temperature	150°C (Continuous)
Actuator Resistance at 25°C	2.6 ± 0.3 Ω
Actuator Inductance at 25°C	14.5 ± 3mH

APPENDIX C. H-BRIDGE MOTOR DRIVER

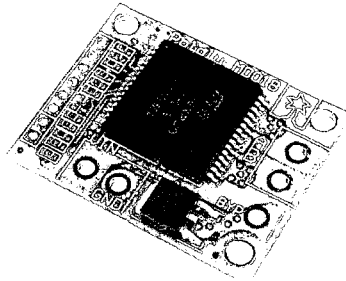


Figure C-1: H-bridge motor driver carrier [29]

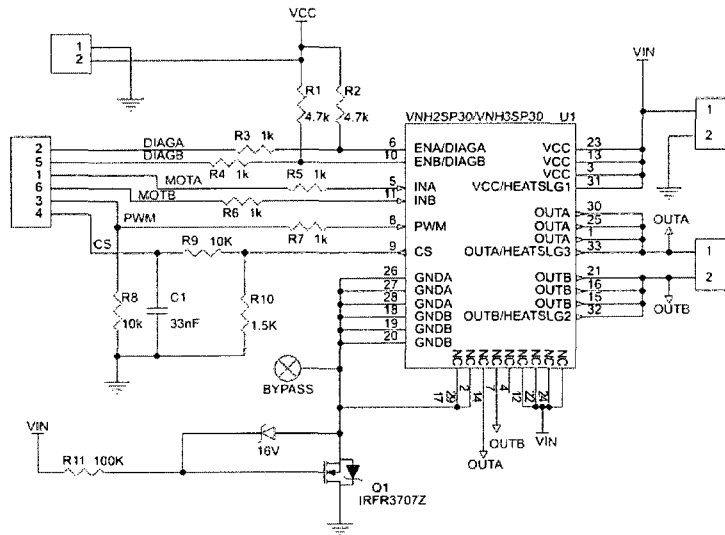


Figure C-2: H-bridge circuit [29]

Table C-1: Specifications of Pololu High-Current Motor Driver Carrier [29]

Model	VNH2SP30 Motor Driver Carrier
Max PWM Frequency	20kHz
Current Sense	Approximately 0.13 Volts/Amp
Over-voltage shutoff	16V (19V typical)
Current for Infinite Run Time	14A
Max Current	30A

The solenoid device operation can be described by three major equations below.

The electrical circuit equation is:

$$U = iR + L \frac{di}{dt} \quad (\text{C.1})$$

The magnetic circuit equation is:

$$iN = \phi_{\delta} \times (2R_{\delta} + R_f + \sum R_m) \approx \phi_{\delta} \times 2R_{\delta} = \phi_{\delta} \times \frac{\delta_0}{\mu_0 S} \quad (\text{C.2})$$

where, $\phi_{\delta} = BS$, δ_0 is the air gap distance, $\mu_0 = 4\pi \times 10^{-7} \text{ H/m}$, S_0 is the affective area.

The electro-magnetic force (EMF) is:

$$F_{avg} = \frac{B_m^2 S}{4\mu_0} \quad (\text{C.3})$$

$$F_{max} = \frac{B_m^2 S}{2\mu_0} \quad (\text{C.4})$$

Therefore, the maximum electro-magnetic force generated is derived as,

$$F_{max} = \frac{B_m^2 S_0}{2\mu_0} = \frac{\left(\frac{\phi_{\delta}}{S_0}\right)^2 S_0}{2\mu_0} = \frac{\left(\frac{iN}{\frac{2\delta_0}{\mu_0 S_0}}\right)^2 S_0}{2\mu_0} = \frac{i^2 N^2 \mu_0 S_0}{8\delta_0^2} \quad (\text{C.5})$$

APPENDIX D. VARIABLE COMPRESSION RATIO (VCR)

Main VCR operating principles are represented in the following scheme:

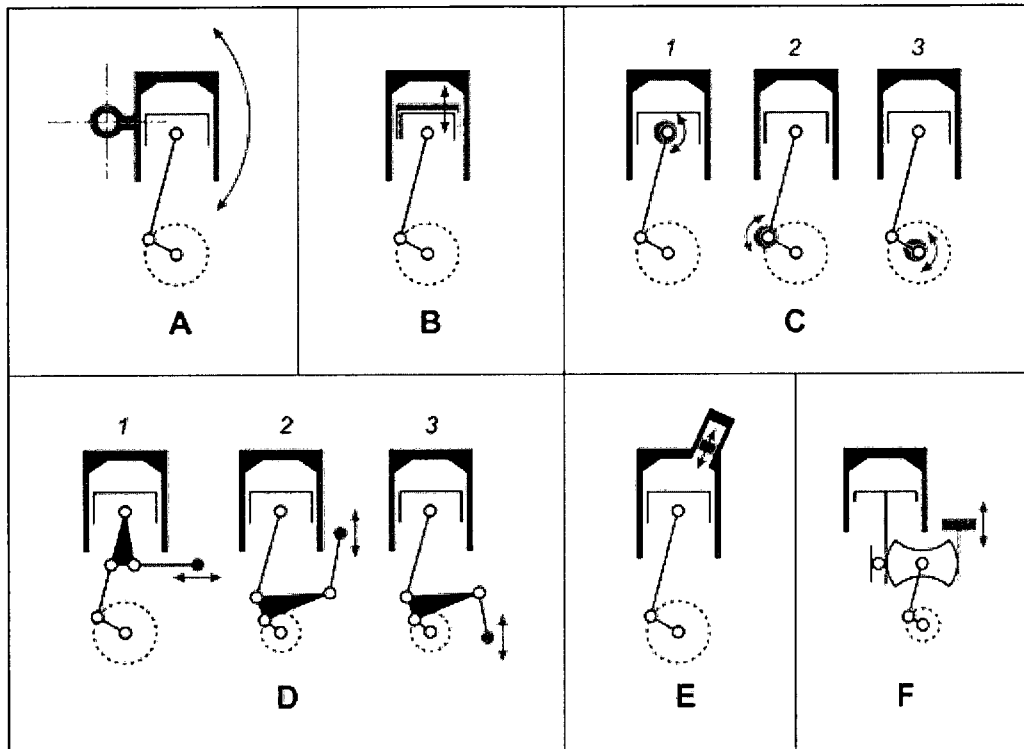


Figure D-1: VCR operating principles [30]

A: Articulated cylinder head

B: Hydraulic pistons

C: Eccentrics on bearings

D: Multilink rod-crank mechanisms

E: Additional piston in cylinder head

F: Gear-based mechanisms

APPENDIX E. VARIABLE VALVE TIMING (VVT)

Variable valve timing (VVT) and the variable length intake manifold (VLIM) are designed to broaden the torque band of the engine.

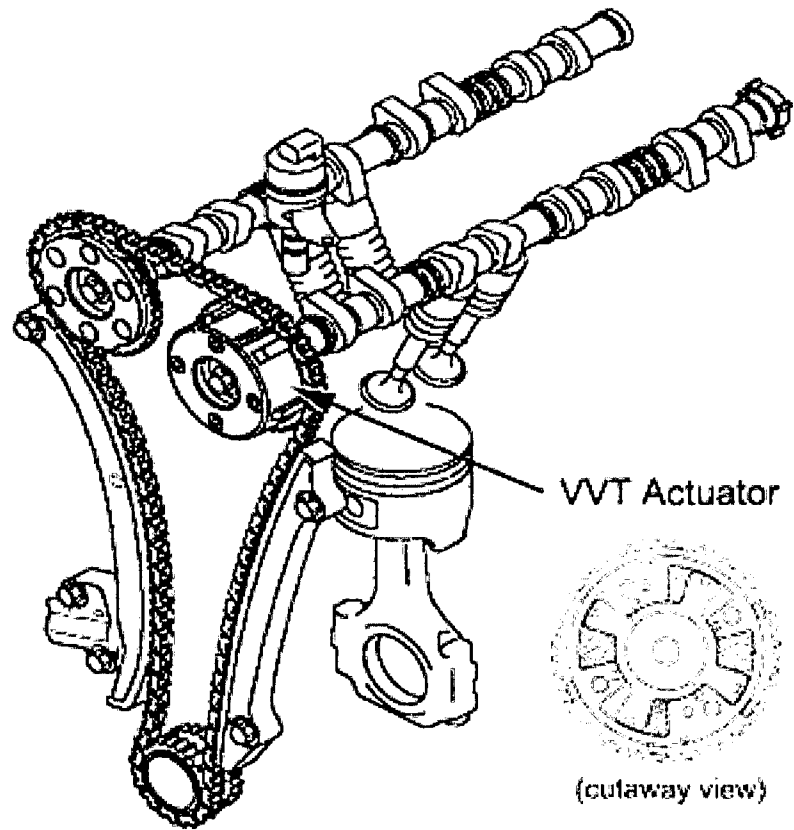


Figure E-1: VVT actuator [31]

APPENDIX F. VARIABLE GEOMETRY TURBOCHARGER (VGT)



Figure F-1: VGT vanes in exhaust flow [32]

The Variable Geometry Turbocharger (VGT) is used for better economy and load response. The “variable” part of the turbo provides performance by electronically positioning exhaust airflow vanes. The vanes are in the exhaust flow. The external actuator has a mechanical linkage to move the vanes to the appropriate position. The opening or closing of the vanes changes the outlet volume and airflow speed against the turbocharger impeller. More specifically, narrow vane openings increase boost at low speed and load while wider vane openings increase efficiency at high speed and load [32].

The ability to keep the airflow going at the optimum point provides more consistent engine boost pressure and the ability to respond to load quickly. Boost pressure in the intake manifold is controlled at its optimum point to provide economy and performance regardless of engine speed or load. Overall, the applying of the VGT results in the increase in the low-speed torque and the peak torque and the improvement in the fuel economy and engine performance at high altitudes. In addition, VGT also allows quicker response to engine load [32].

VITA AUCTORIS

NAME: Yuyu Tan

PLACE OF BIRTH: Tianjin, P.R.China

DATE OF BIRTH: October 19, 1981

EDUCATION: University of Windsor, Windsor, Ontario, Canada
2005-2007, M.A.Sc
Tianjin University, Tianjin, P.R.China
2000-2004, B.Eng.